

# Enhancement of the spin-wave nonreciprocity in antiferromagnetically coupled multilayers with dipolar and interfacial Dzyaloshinskii-Moriya interactions

A. F. Franco *Centro de Investigación DAITA Lab, Facultad de Estudios Interdisciplinarios, Universidad Mayor, Chile*P. Landeros *Departamento de Física, Universidad Técnica Federico Santa María, Avenida España 1680, 2390123 Valparaíso, Chile and Center for the Development of Nanoscience and Nanotechnology (CEDENNA), 917-0124 Santiago, Chile*

(Received 10 June 2020; revised 9 September 2020; accepted 30 October 2020; published 19 November 2020)

Spin-wave-based circuits and logic devices have been considered as an alternative to current electronic devices as they approach the physical limit of miniaturization. Asymmetrical propagation of spin waves, also known as nonreciprocity, provides an additional degree of freedom to these spin-wave-based devices, increasing their flexibility. In thin films, nonreciprocity can be induced by the Dzyaloshinskii-Moriya interaction (DMI) at heavy-metal/ferromagnet bilayers, and by the dipolar coupling in multilayers. Here, we show that in an antiferromagnetically coupled multilayer with interfacial DMI, the frequency nonreciprocity induced by the DMI is enhanced when both heavy metals are the same as long as the multilayer remains in an antiparallel state. Furthermore, we show that the interplay between the dipolar and Dzyaloshinskii-Moriya interaction enhances the nonreciprocity of one oscillation mode and reduces the nonreciprocity of the other. Which mode is enhanced depends on the sign of the induced Dzyaloshinskii-Moriya interaction at the interfaces and the magnetic moments of the layers. Finally, we show that it is possible to change the frequency nonreciprocity of Pt/Co/Cu/Co/Pt and Pt/Co/Cu/Py/Pt multilayers by  $\sim 7$  GHz when applying an in-plane magnetic field of 130 mT. This includes a change in the sign of the nonreciprocity, which could be used to control the direction of the flux of information in spin-wave devices.

DOI: [10.1103/PhysRevB.102.184424](https://doi.org/10.1103/PhysRevB.102.184424)

## I. INTRODUCTION

During recent years, spin-wave (SW)-based circuits and logic devices have been considered as an alternative to overcome the fundamental physical constraints in the scaling of current electronic devices [1–10]. Nonsymmetrical propagation of SWs provide an additional degree of freedom for these devices, potentially increasing their flexibility and applicability, making the topic of nonreciprocity (NR) highly thriving in the current research environment [11–31]. Typically two kinds of NR are observed in magnetic thin films and multilayers: Amplitude NR and frequency NR. In amplitude NR the asymmetry is observed as a change in the SW intensity when propagating in opposite directions (with the same wave vector). It is typically observed in surface SWs propagating perpendicular to the magnetization, configuration typically known as Damon-Eschbach (DE), and depends on the thickness of the layer in such way that disappears for ultrathin films. Here, the SWs propagate in opposite surfaces of a magnetic thin film, and the amplitude NR arises due to the asymmetric localization of the dipole field along the thickness [11,32]. On the other hand, in frequency NR the asymmetry is observed as a change in the frequency of the SWs that propagates in opposite directions, with characteristics that depend on the contributions that induce the NR. Some of these contributions are the Dzyaloshinskii-Moriya interaction (DMI) [33–44], dipolar fields [45–53],

interfacial perpendicular anisotropy [12,19,32], the curvature of the system [54], and light radiation [55]. From these contributions, the interfacial DMI (iDMI), induced when a heavy-metal (HM) layer is in contact with a thin ferromagnetic (FM) layer [56–60] is currently of particular interest due to its capabilities to induce a magnetic texture with an spatial chirality, which depends on the sign of iDMI constant  $D$  [56,57]. This particular characteristic has been exploited to induce skyrmions, bubble domains, chiral domain walls, and biased hysteresis loops in magnetic structures [61–67]. It is in this spatial chirality where the origin of the iDMI-induced frequency NR lies. In FM thin films, the SWs present a spatial chirality that depends on the direction of propagation (given by the wave vector  $\vec{k}$ ) relative to the direction of the magnetization. For example, in the DE configuration the SWs propagating in opposite directions  $\vec{k}^+$  and  $\vec{k}^-$  (with frequencies  $f_k^+$  and  $f_k^-$ , respectively) will have opposite chiralities [40]. Thus, depending on whether the chiralities of the iDMI and the SWs are the same or are opposite, the frequency of the SW is reduced in one direction while it is increased in the other direction, inducing an antisymmetric dispersion. The induced frequency difference defined as  $\Delta f = f_k^+ - f_k^-$  is typically referred to as frequency NR, and depends linearly with  $D$  and  $k$  [37–39]. Moreover, it also depends on the thicknesses of the layers as the iDMI strength decreases with the thickness of the ferromagnet [41], and increases

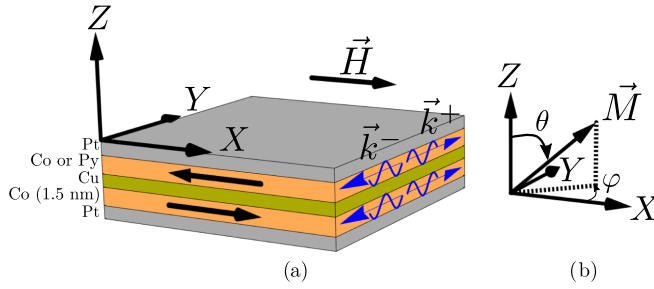


FIG. 1. (a) Scheme of the antiferromagnetically coupled Pt/Co/Cu/(Co or Py)/Pt multilayer and definition of the Cartesian coordinate system. (b) Definition of the spherical coordinate system.

moderately with the thickness of the heavy-metal layer [44]. iDMI-induced frequency NR (iDMI-NR) is also observed in multilayers, which offer additional flexibility on the material combination and structure configuration, while conserving the linear dependence with both  $D$  and  $k$  [62,68].

In addition to the iDMI, it has been shown that the interlayer dipolar coupling (IDC) also can induce frequency NR in multilayer structures [45–47]. More recent studies have used Brillouin light scattering measurements to show IDC-induced frequency NR (IDC-NR) in structures composed of a Ni layer antiferromagnetically coupled to a Py stripe magnonic crystal [49], and have shown theoretically and experimentally that this NR can be controlled by changing the relative direction of the magnetization of the layers, providing the possibility of having reconfigurable devices [51,69].

In this work we show theoretically an enhancement of the iDMI-induced frequency NR in the antiferromagnetically coupled Pt/Co/Cu/(Co or Py)/Pt multilayer shown in Fig. 1(a). As this structure is composed by two magnetic materials, two resonance modes are expected. We calculate the SW frequencies  $f_k^+$  and  $f_k^-$  of these modes, the iDMI-NR, and showcase the interplay with the IDC-NR. We show that their interplay enhances the frequency NR of one resonance mode, while reducing the frequency NR of the other. Moreover, we also show that the contributions of opposite HM/FM interfaces composed of the same materials have additive contributions to the frequency NR when the multilayer has antiparallel magnetization, opposite to what is expected from thin films [62,70,71]. Finally, we propose a configuration of the Pt/Co/Cu/Py/Pt multilayer, which allows us to control the frequency NR by applying a magnetic field, reaching changes in the frequency NR of 7 GHz with fields of 150 mT by changing between parallel (P) and antiparallel (AP) magnetization states, and discuss the conditions under which such changes can be obtained. These results allow for highly reconfigurable nonreciprocal devices with frequency variations that can be tailored by adjusting the respective iDMI and IDC contributions. Finally, note that in this work we focus on frequency NR, and thus from this point onward frequency will be omitted and it will be referred simply as NR.

## II. SYSTEM AND METHODS

The spin-wave dispersion of these multilayers is calculated using a model proposed in Ref. [72], in which the resonance

frequencies  $\omega_{\text{res}} = 2\pi f_{\text{res}}$  are calculated from the Landau-Lifshitz-Gilbert equation. We start from the Hamiltonian of the system (see Refs. [72–74] for detailed expressions), which is then introduced in the Landau-Lifshitz-Gilbert equation. After linearization of the resulting equations of motion, we obtain a set of linear equations (two for each magnetic layer), which can be solved by calculating the eigenvalues of the matrix

$$B_m = \mu_0\gamma \begin{bmatrix} -H_{y_1x_1} & -H_{y_1y_1} & -H_{y_1x_2} & -H_{y_1y_2} \\ H_{x_1x_1} & H_{x_1y_1} & H_{x_1x_2} & H_{x_1y_2} \\ -H_{y_2x_1} & -H_{y_2y_1} & -H_{y_2x_2} & -H_{y_2y_2} \\ H_{x_2x_1} & H_{x_2y_1} & H_{x_2x_2} & H_{x_2y_2} \end{bmatrix}. \quad (1)$$

The fields  $H_{\alpha_i\beta_j}$  depend on the magnetic features of the layers and the equilibrium direction of the magnetization, where  $\alpha, \beta = x, y$ , and  $i, j$  are the indexes representing each individual layer.  $\gamma = 1.76 \times 10^{11} \text{ Ts}^{-1}$  is the gyromagnetic ratio. We are interested in the magnetic states where both magnetizations are along the  $X$  axis, either P or AP to each other. The applied field  $H$  is also taken along the positive  $X$  direction, and the anisotropy induced at the interfaces with the Pt is perpendicular to the plane of the layer ( $Z$  direction). The wave vector  $\vec{k}^\pm$  is taken to be in the plane of the layer, perpendicular to the direction of the magnetization ( $\varphi_k = \pm\pi/2$ , where  $\varphi_k$  is the direction of  $\vec{k}^\pm$  measured from the  $X$  axis, i.e., DE spin waves). We provide expressions for this configuration, and expressions for the general case can be found in Refs. [37,72–74] for the interlayer exchange coupling (IEC), and in Appendix A for the interlayer dipolar coupling.

Similarly, in some cases we need to study the transitional regime where the multilayer changes from antiparallel to parallel states (and viceversa). In order to study this regime, it is necessary to calculate the equilibrium state of the magnetization  $\vec{M}_i^0$ . A description of how this equilibrium state is calculated can be found in the Appendix B.

### A. Individual layer contributions

For each individual ferromagnetic layer  $i$  with saturation  $M_i$ , the dynamical fields are given by Refs. [37,73,74]

$$\begin{aligned} H_{x_ix_i}^I &= \pm H + M_i - H_{K_i} + S_i k^2 - M_i F(kt_i) \\ H_{y_iy_i}^I &= \pm H + S_i k^2 + M_i F(kt_i) \\ H_{x_iy_i}^I &= -H_{y_ix_i}^I = \pm i 2M_i k \lambda_{\text{dmi}}^i \end{aligned} \quad (2)$$

where  $k$  takes positive values for  $\varphi_k = \pi/2$  ( $\vec{k}^+$ ) and negative values for  $\varphi_k = -\pi/2$  ( $\vec{k}^-$ ).  $\pm$  is positive for magnetization along  $+X$ , and negative for magnetization along  $-X$ . The different terms in the first line of (2) represent, respectively, the external field, the demagnetizing energy, the uniaxial anisotropy, the exchange stiffness, and the intralayer dynamical dipolar field. The iDMI contribution is included in  $H_{x_ix_i}^I$  and  $H_{y_ix_i}^I$ . All subindexes  $i, j$  relate to the physical parameters of the layer  $i, j$ , respectively.  $H_{K_i} \equiv 2K_i/(\mu_0 M_i)$  is the perpendicular uniaxial anisotropy field, and  $K_i$  is the magnitude of the anisotropy.  $S_i \equiv 2A_i/(\mu_0 M_i)$ , where  $A_i$  is the exchange stiffness.  $F(x) = 1 - (1 - \exp[-x])/x$ , and  $t_i$  is the thickness. The iDMI parameter  $\lambda_{\text{dmi}}^i$  has length units

and is defined as  $\lambda_{\text{dmi}}^i \equiv 2D_i/(\mu_0 M_i^2)$ , where  $D_i$  is the volume averaged effective iDMI, and is proportional to the strength of the coupling induced at the HM/FM interface, and inversely proportional to the thickness of the FM. The fields composing the matrix (1) are then given by  $H_{\alpha_i\beta_j} = H_{\alpha_i\beta_j}^I + H_{\alpha_i\beta_j}^J + H_{\alpha_i\beta_j}^d$ , where the contribution from the IEC  $H_{\alpha_i\beta_j}^J$  and the IDC  $H_{\alpha_i\beta_j}^d$  are given below.

### B. Interlayer exchange and dipolar interactions

When  $i \neq j$ , contributions from interlayer coupling start to appear. In the general case, we have obtained the fields for the IEC (see supplementary data in Ref. [72]) and the IDC (see Appendix A). For P (and AP) magnetization and DE spin waves, the IEC contribution is given by

$$\begin{aligned} H_{x_i x_i}^J &= H_{y_i y_i}^J = \sum_j \left[ \sigma_{ij} \frac{J_{\text{eff}}^{ij}}{\mu_0 M_i t_i} + \frac{A_s^{ij}}{\mu_0 M_i} k_i^2 \right] \\ H_{x_i x_j}^J &= -\frac{J_{\text{eff}}^{ij}}{\mu_0 M_j t_j} \\ H_{y_i y_j}^J &= \sigma_{ij} \frac{J_{\text{eff}}^{ij}}{\mu_0 M_j t_j} \\ H_{x_i y_j}^J &= H_{y_i x_j}^J = 0. \end{aligned} \quad (3)$$

The summation over  $j$  refers to the neighboring layers  $i+1$  and  $i-1$ .  $\sigma_{ij} = 1$  for P and  $\sigma_{ij} = -1$  for AP magnetization.  $J_{\text{eff}}^{ij}$  is the effective exchange coupling constant between layers  $i$  and  $j$ , and is positive for ferromagnetic coupling and negative for antiferromagnetic exchange, and represents the  $k=0$  contribution of the exchange coupling to the dynamics of the multilayer. The interlayer exchange stiffness  $A_s^{ij}$  contributes to the  $k \neq 0$  dynamics, and is obtained by comparison with the standard exchange stiffness  $A = (nS^2/a)J$  [75]. Using  $t_{\text{Cu}}$  as lattice parameter, and  $n=1$ , we obtain  $A_s^{ij} \equiv J_{\text{eff}}^{ij} t_{\text{Cu}}$ . Note that it gives a contribution on  $k^2$  to the dispersion relation of the system, similar to the exchange stiffness of an individual layer. Thus, NR contribution from the IEC is not expected.

The dynamical ( $k \neq 0$ ) contribution of the IDC for thin films ( $t_i |k| \ll 1$ ) is given by

$$\begin{aligned} H_{x_i x_j}^d &= -M_j \zeta_{\text{idc}}^{i,j} \\ H_{x_i y_j}^d &= i \operatorname{sgn}(Z_j^0 - Z_i^0) M_j \zeta_{\text{idc}}^{i,j} \sin(\varphi_k - \varphi_j) \\ H_{y_i x_j}^d &= i \operatorname{sgn}(Z_j^0 - Z_i^0) M_j \zeta_{\text{idc}}^{i,j} \sin(\varphi_k - \varphi_i), \\ H_{y_i y_j}^d &= \pm M_j \zeta_{\text{idc}}^{i,j} \frac{k}{|k|}, \end{aligned} \quad (4)$$

where

$$\zeta_{\text{idc}}^{i,j} \equiv \frac{1}{t_i |k|} \sinh\left(\frac{t_i |k|}{2}\right) \sinh\left(\frac{t_j |k|}{2}\right) e^{-|k| \Delta Z_j^i}. \quad (5)$$

$\Delta Z_j^i \equiv |Z_i^0 - Z_j^0|$ , and  $Z_i^0$  is the  $Z$  coordinate of the layer  $i$  measured at the center of the layer.  $\operatorname{sgn}(x)$  is the sign function, and  $\varphi_j$  is the in-plane deviation of  $\vec{M}_j$  relative to the  $X$  axis. We do not account for the  $k=0$  contribution of the IDC to the spin wave dispersion, as it is negligible in multilayer systems with lateral sizes much larger than their thicknesses (see Appendix B and Ref. [76]).

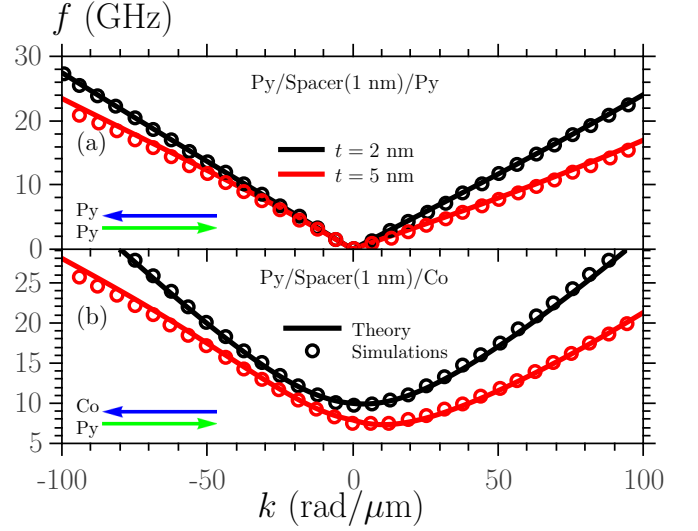


FIG. 2. Dispersion relation of (a) Py( $t$ )/Separator(1 nm)/Py( $t$ ) and (b) Py( $t$ )/Separator(1 nm)/Co( $t$ ) magnetic bilayers with AP magnetization, for thicknesses  $t = 2$  and  $5$  nm. Comparison between theoretical model and micromagnetic simulations from Ref. [51].

With the objective of validating the model, in particular the IDC contribution to the SW frequency, in Fig. 2 we show a comparison between theoretical calculations from our model and the simulations performed by Gallardo *et al.* [51] for Py/Py and Py/Co magnetic bilayers with AP magnetization. The physical parameters are the same used within the reference, excepting  $A_s^{ij}$ , which is taken as zero independent of the value of  $J_{\text{eff}}^{ij}$ . In all cases a good agreement between the two results can be observed, with slight deviation being observed for high negative  $k$  in the case of  $t = 5$  nm. This is expected, as the expressions given in Eq. (4) assume thin films, and become less precise as  $k$  and/or  $t$  increases.

Before advancing with the obtained results, we will briefly discuss the physical parameters used within this work, which are included in the Table I from Appendix C. In particular, it is necessary to differentiate between the Co/Pt interfaces at opposite sides the multilayer, as they are not necessarily identical [70,71]. Thus, throughout this paper Pt/FM refers to the bottom interface, and FM/Pt refers to the top interface, and their physical parameters are differentiated accordingly. Moreover, in all cases the demagnetizing energy is stronger than the perpendicular anisotropy, and thus in-plane magnetization is obtained. Additionally, and for easier reference, Table II from Appendix C shows a list of abbreviations and mathematical symbols commonly used throughout the discussions within the paper.

### III. FREQUENCY NONRECIPROCITY IN THE COUPLED MULTILAYER

In this section we will calculate the frequency NR of a Pt/Co(1.5)/Cu/Co(1.5)/Pt multilayer with AP magnetization, where the thicknesses of the magnetic films are given in nm. We focus first on the separate contributions of the iDMI-NR and IDC-NR, and then on the interplay between them.

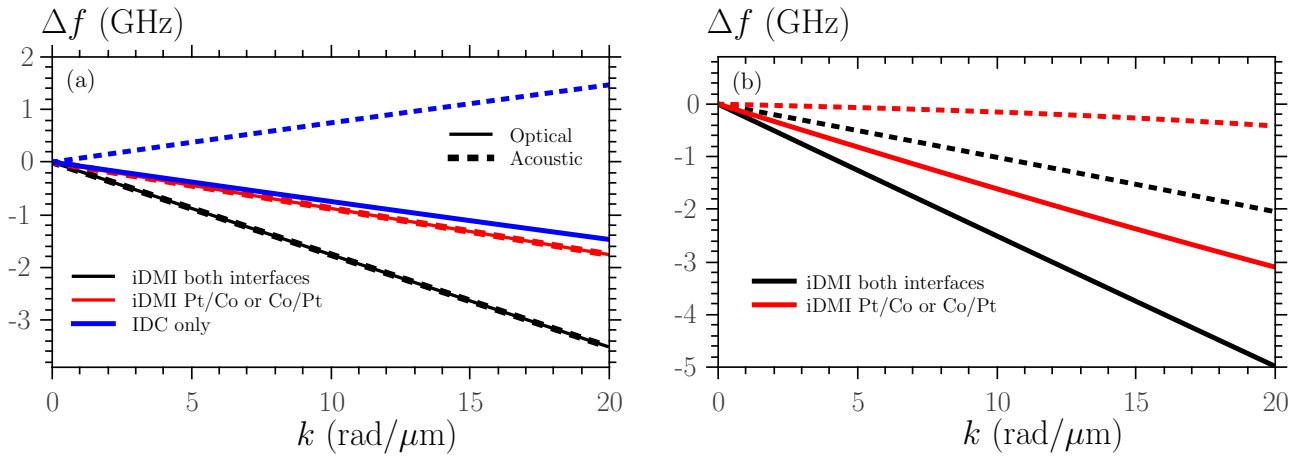


FIG. 3. (a) Frequency nonreciprocity from interfacial Dzyaloshinskii-Moriya interaction and (b) total frequency nonreciprocity of Damon-Eshbach spin waves in an antiferromagnetically coupled Pt/Co(1.5)/Cu/Co(1.5)/Pt multilayer as function of  $k$ . Interfacial Dzyaloshinskii-Moriya interaction is induced in a single or in both Co interfaces, and identical Pt/Co and Co/Pt interfaces are assumed.

Furthermore, the contribution of the Pt/Co and Co/Pt to the iDMI-NR are studied separately with the objective of better understanding the observed behavior of the spin waves. This is performed for two configurations of the multilayer: First, an approach where the bottom and top interfaces are identical, which allows us to observe an enhancement of the iDMI-NR due to additive contributions of the iDMI at opposite interfaces. Second, both interfaces are assumed non-identical [70,71], and thus each has different contributions to the magnetization behavior. Finally, and for completeness, in Appendix D we discuss the behavior of the NR of a Pt/Co(1.5)/Cu/Co(2)/Pt multilayer as function of the effective IEC.

Before presenting our results, we will discuss briefly the oscillation modes of antiferromagnetically coupled bilayers. In the parallel state, the acoustic (uniform precession) and optical (antiphase precession) modes have a higher and lower frequency, respectively. If the system is in an AP state, the relative precession of the layers depends on the applied field and  $J_{\text{eff}}$  [72,81], and it becomes difficult to characterize the modes as either acoustic or optical based on their in-phase or antiphase precession. Throughout this work we refer to the low-frequency mode as optical and to the high-frequency mode as acoustic regardless of the orientation of the magnetization. This is consistent with the well-defined in-phase or antiphase precession observed for P magnetization. Furthermore, the frequency nonreciprocity of the optical and acoustic modes will be referred to as optical NR and acoustic NR, respectively.

## A. Identical Pt/Co and Co/Pt interfaces

### 1. Nonreciprocity induced by the interfacial Dzyaloshinskii-Moriya and dipolar interactions

Figure 3(a) shows the NR as function of  $k$  in a Pt/Co(1.5)/Cu/Co(1.5)/Pt structure, assuming identical Pt/Co and Co/Pt interfaces using the physical parameters presented in Table I. We show the NR when iDMI is induced at a single interface (red), or at both interfaces (black), and the isolated IDC-NR (blue). Note that the same iDMI-NR is obtained

whether Pt/Co or Co/Pt is taken as both interfaces are identical. Figure 3(a) also shows an increase of the iDMI-NR when iDMI is induced at both interfaces. It can be observed that the iDMI-NR is double that in the single interface case, which means that in a multilayer with AP magnetization, the positive and negative iDMI induced at opposite interfaces do not cancel each other out (as it would be expected in single thin films and bilayers with P magnetization), and have additive contributions instead.

To explain this effect we use Fig. 4, which describes schematically the effect of the relative orientation of the magnetization and the sign of  $D$  on the frequency of SWs propagating in opposite directions in a DE configuration. For a single layer with negative  $D$ ,  $f_k^+$  decreases and  $f_k^-$  increases, leading to a negative NR [Fig. 4(a)]. This is the case of, e.g., Pt/Co bilayers [42]. If we stay in the same reference frame and invert the direction of the magnetization,  $f_k^+$  increases and  $f_k^-$  decreases as long as  $D < 0$ , thus the sign of the NR changes [Fig. 4(b)]. Changing the sign of  $D$  causes a second change in the sign of the iDMI-NR, making it negative again [Fig. 4(c)]. Finally going back to the original orientation of the magnetization while keeping a positive  $D$  induces a positive NR [Fig. 4(d)]. In the identical Pt/Co/Cu/Co/Pt multilayer, the bottom Co has magnetization along positive  $X$  and negative  $D$ , thus is described by Fig. 4(a). Similarly, the top Co has magnetization along negative  $X$  and positive  $D$ , and thus is described by Fig. 4(c). This leads to a situation where  $f_k^+$  decreases in both layers and  $f_k^-$  increases in both layers, inducing additive contributions from opposite interfaces, effectively increasing the iDMI-NR of the whole structure. Finally, Fig. 3(a) also shows that the optical and acoustic IDC-NR have the same magnitude, but opposite signs (solid and dashed blue lines).

### 2. Interplay between the interfacial Dzyaloshinskii-Moriya and the dipolar interactions

Figure 3(b) shows the total NR (accounting for the contributions of the iDMI and IDC) when iDMI is induced at a single interface (red lines) or at both interfaces (black lines).

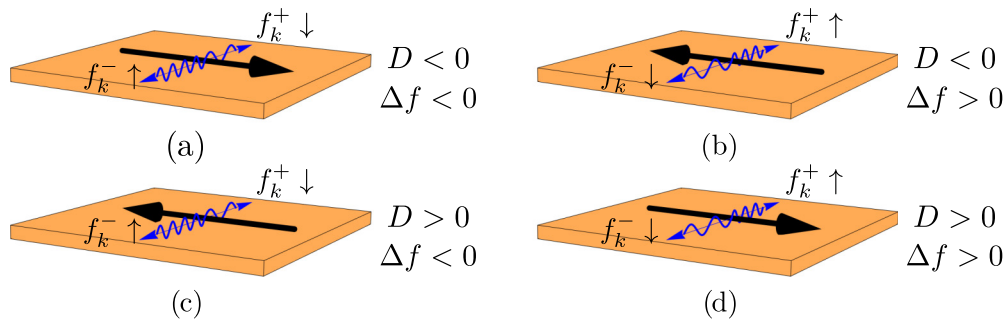


FIG. 4. Effect of the relative orientation of the magnetization and the sign of  $D$  on the frequency of Damon-Eshbach spin waves propagating in opposite directions ( $f_k^\pm \uparrow$ : frequency of  $\vec{k}_\pm$  increases,  $f_k^\pm \downarrow$ : frequency of  $\vec{k}_\pm$  decreases) in a single film.

When comparing to the results shown in Fig. 3(a), an additive interplay between both NR contributions can be observed. Because the acoustic iDMI-NR and IDC-NR have opposite signs, the total acoustic NR decreases in magnitude. On the other hand, the optical iDMI-NR and IDC-NR are both negative, and thus the total optical NR increases in magnitude. Changing the Pt to, e.g., Ir at both interfaces induces a  $D$  with opposite sign [62,82], and changes the sign of the iDMI-NR, enhancing the acoustic NR instead of the optical.

## B. Nonidentical Pt/Co and Co/Pt interfaces

### 1. Governing layers of the oscillation modes

Taking into account that the Pt/Co and Co/Pt interfaces are not necessarily identical [70,71], we also study the case where the top and bottom Co layers in a Pt/Co(1.5)/Cu/Co(1.5)/Pt multilayer differ in  $D$  and  $K$ . While  $D$  only affects the  $k \neq 0$  case,  $K$  does affect the base resonance frequency of the layers. In particular, the resonance frequency of the Co thin films depends on the difference  $M_i - H_{K_i}$  [first line of (2)]. This difference is smaller in bottom Co (240 kA/m) compared to the top Co (1320 kA/m), and as consequence the bottom Co has a lower natural resonance frequency than the top Co. Moreover, as discussed previously, in an AFM coupled bilayer the optical mode has a lower frequency than the acoustic mode. In previous works we have shown that these modes are governed by the layers with closest natural resonance

frequency, i.e., the low-frequency mode is governed by the layer with lowest natural resonance frequency, and the high-frequency mode is governed by the layer with highest natural resonance frequency [72]. As a consequence, the optical mode is mostly governed by the bottom Co (low frequency), and the acoustic is governed by the top Co (high frequency).

### 2. Nonreciprocity of the optical and acoustic oscillation modes

Figure 5 shows the relation dispersion and the NR of the Pt/Co(1.5)/Cu/Co(1.5)/Pt multilayer as function of  $k$ . Figure 5(a) shows the SW dispersion, while Fig. 5(b) shows the iDMI-NR, the IDC-NR, and the combination of both. Figure 5(a) clearly shows NR in all presented cases. This NR is better illustrated in Fig. 5(b), where the different contributions to  $\Delta f$  can be clearly differentiated, and we can conclude the following:

(i) The nonreciprocity induced by the interlayer dipolar coupling again have the same magnitude for the optical and acoustic modes, but opposite signs (solid and dashed blue lines).

(ii) The nonreciprocity induced by the interfacial Dzyaloshinskii-Moriya interaction is negative for both the optical and acoustic modes (red lines), but the optical nonreciprocity is stronger.

Because  $D$  is stronger at the Pt/Co interface when compared to the Co/Pt, we observe a stronger optical iDMI-NR

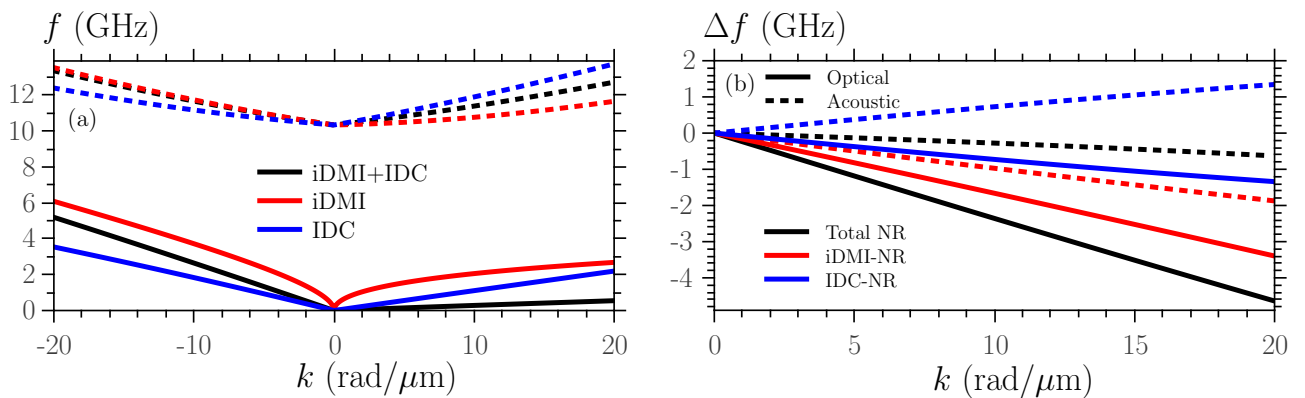


FIG. 5. Frequency behavior of Damon-Eshbach spin waves in an antiferromagnetically coupled Pt/Co(1.5)/Cu/Co(1.5)/Pt multilayer as function of  $k$ , accounting for nonidentical Pt/Co and Co/Pt interfaces. (a) Frequency of spin waves propagating in opposite directions and effect of the interactions. (b) Frequency nonreciprocity from interlayer dipolar coupling, interfacial Dzyaloshinskii-Moriya interaction, and the interplay between the two.

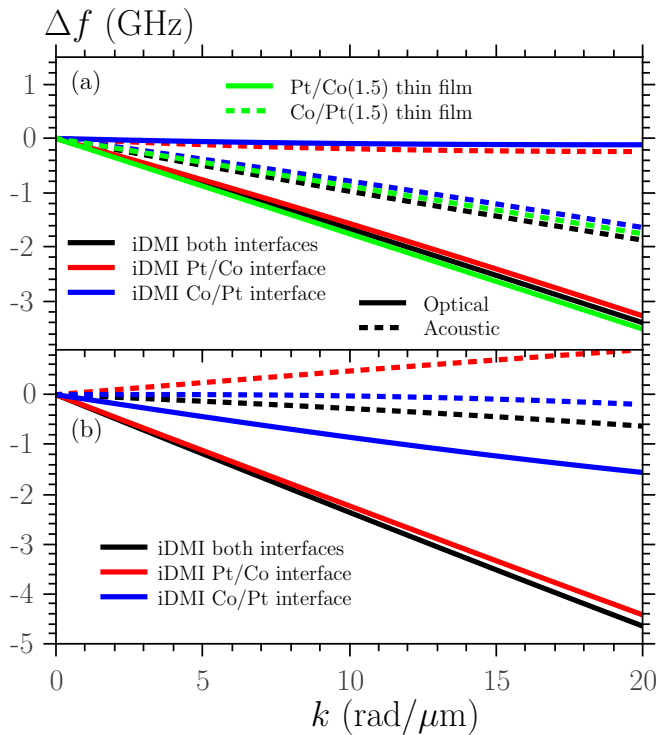


FIG. 6. Frequency nonreciprocity of Damon-Eshbach spin waves in an antiferromagnetically coupled Pt/Co(1.5)/Cu/Co(1.5)/Pt multilayer as function of  $k$ . Interfacial Dzyaloshinskii-Moriya interaction is induced in a single or in both Co interfaces, taking into account nonidentical Pt/Co and Co/Pt interfaces. (a) Frequency nonreciprocity induced only by the interfacial Dzyaloshinskii-Moriya interaction and (b) frequency nonreciprocity taking into account the contributions of the interfacial Dzyaloshinskii-Moriya interaction and the interlayer dipolar coupling.

(bottom Co governs optical mode), and a weaker acoustic iDMI-NR (top Co governs acoustic mode). When both interactions are accounted for (black lines), additive contributions are observed again, and thus the optical NR is enhanced (iDMI-NR and IDC-NR have the same sign), while the acoustic NR is reduced (iDMI-NR and IDC-NR have opposite signs).

### 3. Nonreciprocity induced by interfacial Dzyaloshinskii-Moriya interaction in single interfaces

Figure 6 shows the contribution of the different Pt/Co and Co/Pt interfaces to the iDMI-NR and total NR. Figure 6(a) shows the iDMI-NR when the multilayer has iDMI at the top, at the bottom, or at both interfaces. In order to better understand the contribution of each interface, initially the IDC-NR is not accounted for. When iDMI is induced only at the bottom (red), the optical NR is similar to that of an individual Pt/Co(1.5) thin film, while the acoustic NR is practically nonexistent. This is again because the bottom Co governs the optical mode. The opposite behavior is observed when iDMI is induced only at the top interface (blue), i.e., the acoustic NR is strong while the optical NR is almost zero. Furthermore, the acoustic NR is very similar to that of a single Co(1.5)/Pt structure. However, note that both ferromagnetic layers are

precessing in all modes, hence the NR of each mode would also be present in both layers. This means that it is possible to induce a strong NR in a ferromagnetic thin film by coupling it to a Pt/Co or a Co/Pt structure.

### 4. Contribution of both interfaces to the nonreciprocity

In Fig. 6(a), when iDMI is induced at both interfaces (black), a strong NR is induced in both modes. Moreover, these NRs increase slightly when compared to that of single interfaces because now the weak contribution of one interface is added to the strong contribution of the opposite interface. Additionally, the NR of both resonant modes are very similar to those of individual thin films (green).

Figure 6(b) shows the NR when IDC-NR is accounted for. In all cases the optical NR became more negative and the acoustic NR became more positive due to the additive contribution of the IDC-NR to each mode.

Comparing these results with those shown in Fig. 3 for identical Pt/Co and Co/Pt interfaces we can observe certain similarities as well as some differences. First, in all cases the total acoustic NR is more positive than the total optical NR. However, the single interface contributions to the iDMI-NR vary greatly. This is due not only to the values of  $D$ , but also to the natural (noninteracting) resonance frequencies of the layers. If the natural resonance frequency of both layers is equal (or very similar), the interfaces tend to see the whole structure as a single thin film of thickness  $t_1 + t_2$  [68], thus obtaining the same iDMI-NR when inducing iDMI at opposite interfaces [Fig. 3(a)]. As the difference between the natural frequencies increases, the layer neighboring the interface becomes more relevant, while the opposite layer becomes less relevant, thus reaching the results shown in Fig. 6(a), where the iDMI-NR is closer to that of individual layers.

## IV. RECONFIGURATION OF THE FREQUENCY NONRECIPROcity

Now that the contributions of the different interactions and interfaces are understood, we will take advantage of the antiferromagnetic interlayer exchange coupling to control the nonreciprocity for different configurations of the multilayer. An in-plane external magnetic field is applied to change reversibly the orientation of the magnetization, which in turn induces variations of the NR. By designing appropriately the interplay between the iDMI-NR and the IDC-NR, we show it is possible to obtain reversible variations of the NR as high as  $\approx 7$  GHz with fields as low as 130 mT.

### A. System-1: Pt/Co(1.5)/Cu/Co(1.5)/Pt with nonidentical interfaces

#### 1. Nonreciprocity as function of the applied magnetic field

Figures 7(a)–7(c) show the different dynamic behaviors of an antiferromagnetically coupled Pt/Co(1.5)/Cu/Co(1.5)/Pt multilayer as function of the in-plane external field, accounting for nonidentical anisotropies and DMI at the Pt/Co and Co/Pt interfaces. Figure 7(a) shows the NR, Figure 7(b) shows the frequencies for SWs propagating in both directions, and Fig. 7(c) shows the equilibrium state of the magnetization. In the latter we can observe that at weak fields, both

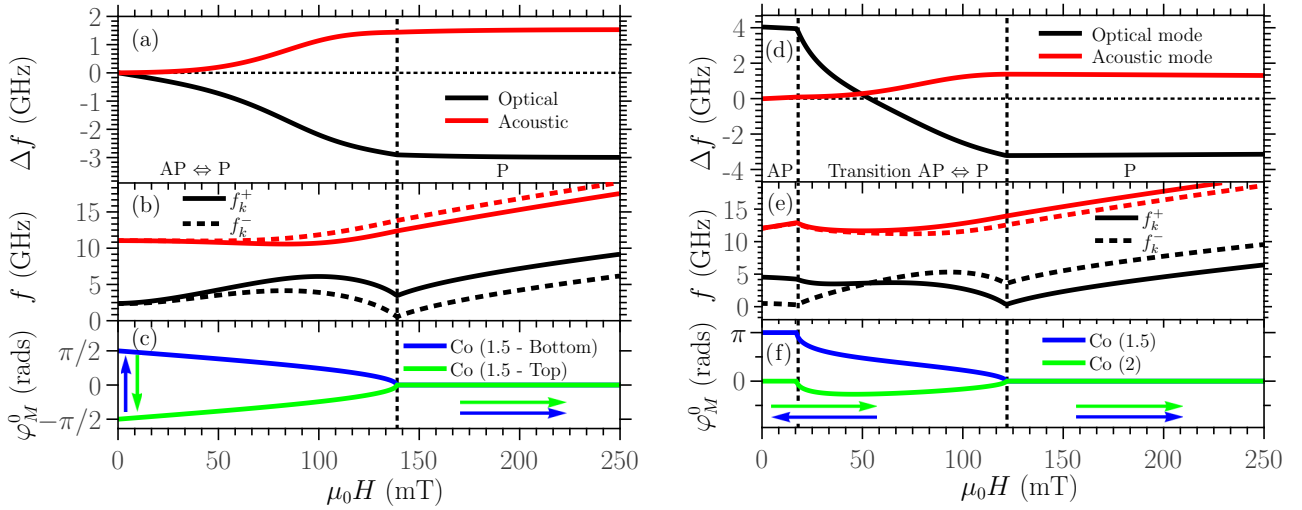


FIG. 7. Behavior of the magnetization of (a)–(c) Pt/Co(1.5)/Cu/Co(1.5)/Pt and (d)–(f) Pt/Co(1.5)/Cu/Co(2)/Pt multilayers as function of the in-plane applied field, with fixed wave vector  $k = 16.7 \text{ rad}/\mu\text{m}$ . (a), (d) Frequency nonreciprocity, (b), (e) frequency of spin waves propagating in opposite directions, and (c), (f) equilibrium orientation of the magnetization.

magnetizations are collinear with  $\vec{k}^\pm$ , and thus both the iDMI-NR and the IDC-NR are zero. As the field increases, the NR of both modes also increases, stabilizing after the multilayer saturates in the  $+X$  direction. In this case, we observe a reversible variation of  $\approx 3 \text{ GHz}$  in the optical NR and  $\approx 1.5 \text{ GHz}$  in the acoustic NR for fields between 0 and 140 mT.

This behavior is observed because at weak fields the competition between the applied field and the AFM IEC aligns the magnetization of the layers in a backward volume AP configuration along the  $\pm Y$  directions (SWs propagate parallel to the magnetization). Thus, the NR becomes zero because the SWs and magnetization are collinear [37,51]. As the field increases it overcomes the effect of the exchange coupling and aligns both magnetizations along the  $+X$  direction, going back to DE configuration and thus inducing a nonzero NR, originating the observed variation.

## B. System-2: Pt/Co(1.5)/Cu/Co(2)/Pt with nonidentical interfaces

### 1. Nonreciprocity as function of the applied magnetic field

With the objective of enhancing the variation of the NR, we increase the thickness of the top Co from 1.5 nm to 2 nm. The results are shown in Figs. 7(d)–7(f), which show different frequency behaviors of the multilayer as function of the in-plane external field. Figure 7(d) shows the NR, Figure 7(e) shows the frequencies for opposite wave vectors, and Fig. 7(f) shows the equilibrium state of the magnetization. In the latter we can observe three different regimes: (i) AP regime, (ii) AP  $\Leftrightarrow$  P transition, and (iii) P regime. These three regimes can also be clearly identified in the NR shown in Fig. 7(d). In the P and AP regimes the NR of both modes tends to remain constant, while the intermediate regime presents a smooth transition. The acoustic NR shows a (reversible) variation of  $\approx 1.5 \text{ GHz}$  when going from AP to P state. On the other hand, the optical NR shows a much higher variation of  $\approx 7 \text{ GHz}$ , showcasing

the possibility of inducing strong changes in the NR with applied fields as low as 130 mT.

### 2. Orientation of the magnetization as function of the applied field

In order to better understand the origin of the large variation of the optical NR, we first need to discuss the three different field regimes and their related magnetization states. At weak fields [regime (i)], the layer with higher magnetic moment [Co(2)] remains aligned to the field. The antiferromagnetic IEC forces the other layer [Co(1.5)] to remain against the applied field, thus reaching an AP state. For intermediate fields [regime (ii)], the applied field starts to overcome the effect of the IEC, and induces changes in the orientation of the Co(1.5). These changes also induce slight deviations in the orientation of the Co(2) because the antiferromagnetic IEC tries to avoid the P state. For strong fields [regime (iii)], the system is saturated in a parallel state.

### 3. Giant variation of the nonreciprocity

Now we will discuss the  $\approx 7 \text{ GHz}$  variation of the optical NR shown in Fig. 7(d). With the objective of better understanding this behavior, we show in Fig. 8 the IDC-NR and iDMI-NR as function of the in-plane external field for the Pt/Co(1.5)/Cu/Co(2)/Pt multilayer.

*a. Nonreciprocity induced by the interlayer dipolar coupling.* Figure 8(a) shows the IDC-NR, where it is evident that the two modes are symmetric around  $\Delta f = 0$  for all values of the applied field. This is because the reciprocity theorem applies to the dipolar interaction, i.e., the energy originated from the dipolar field of the Co(2) acting on the Co(1.5) is equal to the energy originated from the dipolar field of the Co(1.5) acting on the Co(2).

*b. Nonreciprocity induced by the interfacial Dzyaloshinskii-Moriya interaction.* Figure 8(b) shows the iDMI-NR, where a nonsymmetric evolution of the optical and acoustic NR can be observed. This is because the iDMI affects mostly one layer, and its effect is then transmitted to the neighboring layers

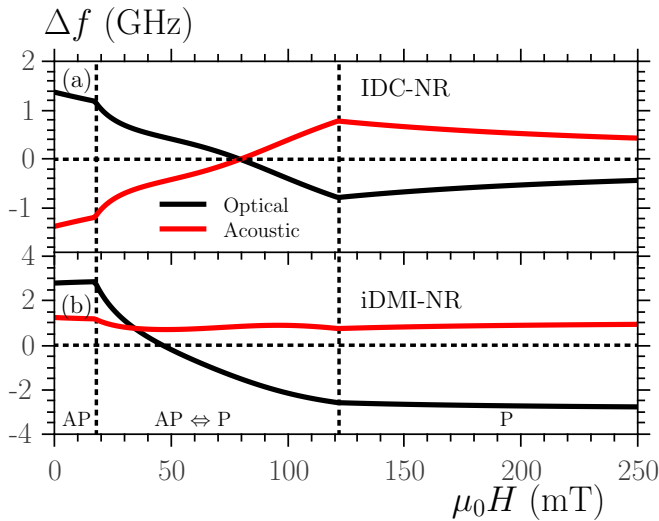


FIG. 8. Frequency nonreciprocity for an antiferromagnetically coupled Pt/Co(1.5)/Cu/Co(2)/Pt multilayer as function of the applied field, and fixed wave vector  $k = 16.7 \text{ rad}/\mu\text{m}$ . Contributions from (a) interlayer dipolar coupling and (b) interfacial Dzyaloshinskii-Moriya interaction.

through the IEC. These resonance modes are mostly governed by the layer with closest natural resonance frequency, i.e.:

- (i) The optical mode is governed by the Co(1.5) due to its lower natural frequency.
- (ii) The acoustic mode is governed by the Co(2) due to its higher natural frequency.

Thus, the iDMI energy of each interface is reflected as a different NR for each mode. As the field increases, the optical iDMI-NR tends toward negative values because the Co(1.5) is changing from an AP to P state. This changes the sign of the optical iDMI-NR [associated mostly to the Pt/Co(1.5) interface], and induces the steep change observed during the transitional AP  $\Leftrightarrow$  P regime. Increasing the field beyond  $\mu_0 H \approx 122 \text{ mT}$  stabilizes the NR of both acoustic and optical modes. On the other hand, the acoustic NR remains mostly constant because the magnetization of the Co(2) remains mostly fixed in the  $+X$  direction.

*c. Interplay between the interfacial Dzyaloshinskii-Moriya and the dipolar interactions.* Due to the relative orientation of the magnetization and the sign of  $D$  at the Pt/Co(1.5) interface, the optical iDMI-NR and optical IDC-NR are both positive when the magnetizations are AP, and both negative when the magnetizations are P, enhancing the optical NR in both cases. This induces a large change in the NR when the magnetization of the Co(1.5) changes orientation.

#### 4. Optimization of the nonreciprocity variation:

##### Detailed discussion

To attain the most optimal variation on the NR, it is necessary to ensure that the iDMI-NR and IDC-NR have the same signs in both AP and P configuration.

*a. Sign of the nonreciprocity induced by the interfacial Dzyaloshinskii-Moriya interaction.* The sign of the iDMI-NR depends on the sign of  $D$  and the orientation of the magneti-

zation, as indicated in the discussion of Fig. 4, and taking into account which mode is governed by each layer.

*b. Sign of the nonreciprocity induced by the interlayer dipolar coupling.* The acoustic and optical IDC-NR in a magnetic bilayer always have the same magnitude but opposite sign. Assuming again DE SWs propagating in the  $\pm Y$  direction, the IDC-NR of a given mode is negative (positive) if the magnetization of the layer governing said mode is in the  $+X$  ( $-X$ ) direction. This rule will always be fulfilled by both ferromagnets in a magnetic bilayer with AP magnetization. However, when the bilayer is in P configuration, the condition that the IDC-NR of both modes have opposite sign takes priority, and thus the IDC-NR of the modes will have opposite sign as expected because the other mode is dominant.

*c. Dominant mode of the interlayer dipolar coupling.* The dominant mode will be the one governed by the layer on which a stronger interlayer dipolar field is acting. From (4), we can see that this field is proportional to the saturation of the other layer ( $M_j$ ), and inversely proportional to the thickness of the current one ( $t_i$ ). This is equivalent to say that the stronger field acts on the layer with lowest  $M_i t_i$  product, thus becoming the dominant one. In the results presented in Figs. 7(d) and 8(a), both layers have the same  $M$ , but the bottom layer (which governs optical mode) is thinner, and thus is the dominant one. Thus, at weak fields the optical IDC-NR is positive (the governing layer points in the  $-X$  direction) and the acoustic IDC-NR is negative (the governing layer points in the  $+X$  direction). When the field increases and induces switching of the magnetization of the (dominant) bottom Co layer, and thus the sign of the optical IDC-NR changes. In consequence, the sign of the acoustic IDC-NR also changes.

*d. Interplay between both interactions.* In the results presented in Figs. 7(d) and 8, the bottom Co has negative  $D$  and points in the  $-X$  direction, which induces a positive optical iDMI-NR at weak fields. Similarly, the bottom Co induces a positive optical DMI-NR, thus ensuring that both optical iDMI-NR and IDC-NR have the same sign (positive) at weak fields, enhancing the total optical NR.

When the field increases and the magnetization of the bottom Co layer switch towards the  $+X$  direction, inducing a change of sign in both the optical iDMI-NR and the optical IDC-NR, again enhancing the total (negative) NR for strong fields, thus ensuring that NR contributions of both interactions have the same sign for both AP and P orientations.

### C. System-3: Pt/Co(1.5)/Cu/Py(1.5)/Pt

#### 1. Nonreciprocity as function of the applied magnetic field

A different behavior can be induced if Py is used instead of Co for the top magnetic layer. In this case, a weaker  $D$  of opposite sign is induced. Figures 9(a)–9(c) show the obtained results as function of the in-plane applied field. Figure 9(a) shows the NR, and a variation of  $\approx 2.5 \text{ GHz}$  has been induced in the acoustic NR, while a maximum variation of  $\approx 2.2 \text{ GHz}$  is induced in the optical NR.

Figure 9(c) shows the equilibrium direction of the magnetization, where we can observe that at weak fields, the Co stays aligned with the field while the Py stays antiparallel due to the higher magnetic moment of the Co. Moreover,  $M_{\text{Py}} - H_K^{\text{Py}} = 362 \text{ kA/m}$ , thus the Py has a higher natural

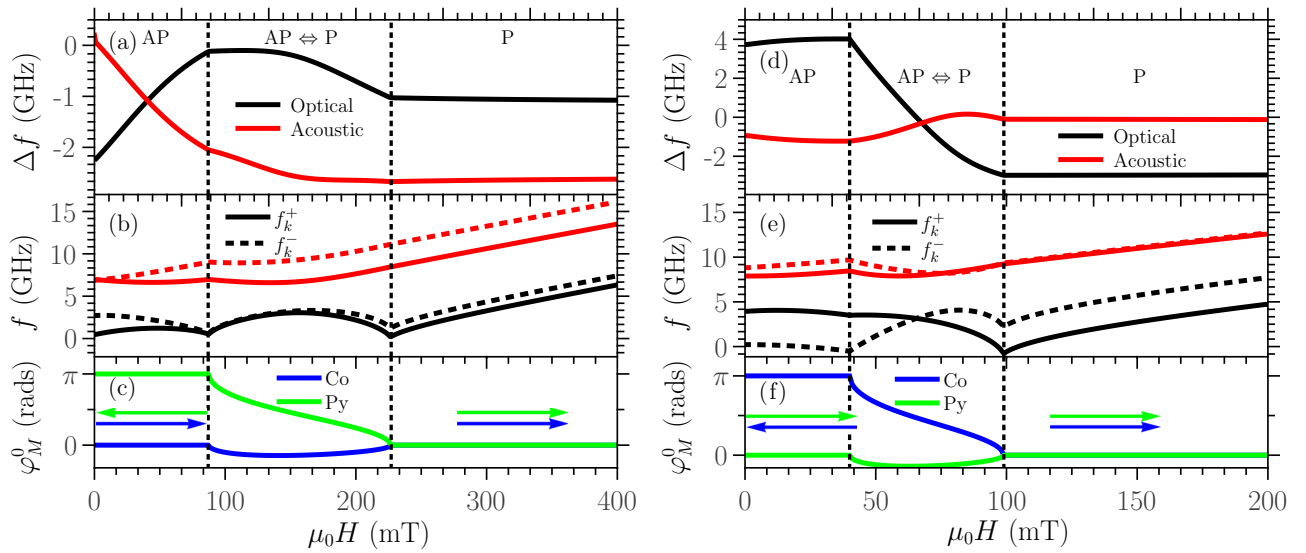


FIG. 9. Behavior of the magnetization of (a)–(c) Pt/Co(1.5)/Cu/Py(1.5)/Pt and (d)–(f) Pt/Co(1.5)/Cu/Py(8)/Pt multilayers as function of the in-plane applied field, with fixed wave vector  $k = 16.7 \text{ rad}/\mu\text{m}$ . (a), (d) Frequency nonreciprocity, (b), (e) frequency of spin waves propagating in opposite directions, and (c), (f) equilibrium orientation of the magnetization.

resonance frequency than the Co. This means that the Py governs the acoustic mode while the Co governs the optical mode. In this situation the iDMI-NR, the IDC-NR, and their interplay behaves as follows:

(i) Because  $D_{\text{Co}}$  is stronger than  $D_{\text{Py}}$ , the sign of the nonreciprocity induced by the interfacial Dzyaloshinskii-Moriya interaction is given by the Co in both modes, and thus this nonreciprocity is negative.

(ii) The nonreciprocity induced by the interlayer dipolar coupling is negative for the optical mode and positive for the acoustic mode.

(iii) Due to the sign of the contributions of each interaction, the total nonreciprocity of the optical mode is enhanced, and that of the acoustic mode decreases.

Increasing the field causes the Py magnetization to switch towards the  $+X$  direction, reaching a P configuration. In this case, the following behavior is observed:

(i) The sign of the nonreciprocity induced by the interfacial Dzyaloshinskii-Moriya interaction does not change because the Co does not change direction.

(ii) The nonreciprocity induced by the interlayer dipolar coupling of both modes changes sign because the dominant layer (Py) changed direction.

(iii) The total nonreciprocity of the acoustic mode is enhanced (both contributions are negative), while that of the optical mode decreases (both contributions have opposite sign).

#### D. System-4: Pt/Co(1.5)/Cu/Py(8)/Pt

##### 1. Nonreciprocity as function of the applied magnetic field

Figures 9(d)–9(f) show the results as function of the applied field after increasing the thickness of the Py layer to 8 nm. A similar behavior to that observed in Fig. 8 for the Pt/Co/Cu/Co(2)/Pt structure is obtained. Figure 9(d) shows the NR, where a variation of  $\approx 7 \text{ GHz}$  can be observed in the

optical NR when the structure goes from AP to P configuration (and vice versa).

Figure 9(f) shows the equilibrium orientation of the magnetizations, and it can be observed that the Co layer remains against the field at weak fields, and switches towards the  $+X$  direction for P configuration. This means that:

(i) The frequency nonreciprocity induced by the interfacial Dzyaloshinskii-Moriya interaction (which is still governed mostly by the Co) changes from positive to negative when increasing the field.

(ii)  $M_{\text{Py}}t_{\text{Py}} > M_{\text{Co}}t_{\text{Co}}$ , and thus the Co (which governs the optical mode) dominates the nonreciprocity induced by interlayer dipolar coupling.

(iii) From the previous point, at weak fields the nonreciprocity induced by interlayer dipolar coupling is positive for the optical mode, and negative for the acoustic. At strong fields, the signs switch as the Co switches direction.

Consequently, both in AP and P configuration the optical NR contributions have the same sign, while the acoustic NR contributions have opposite sign, inducing an enhanced variation of the optical NR as the Co changes direction.

#### E. Typical configuration for optimizing the variation of the nonreciprocity

As summary, we present here typical system configurations, which present the large variation of the optical NR observed in this work:

(i) The basic system is composed of two ferromagnetic thin films separated by a paramagnetic layer.

(ii) Interfacial Dzyaloshinskii-Moriya interaction needs to be induced in at least one ferromagnet. Better results are obtained if it is induced in both ferromagnets. This interaction is typically induced by including a heavy-metal thin film at the external interfaces.

(iii) Thicknesses of the ferromagnetic layers should be between 1–10 nm to maximize the effect of the interfacial

Dzyaloshinskii-Moriya interaction, and to ensure homogeneous spin waves throughout the thickness.

(iv) Antiferromagnetic interlayer exchange coupling should be induced between the ferromagnets. This can be controlled by the thickness of the paramagnetic separator (typically between 0–1.5 nm).

(v) Different saturation\*thickness product ( $Mt$ ) for each ferromagnet.

(vi) The ferromagnet with lowest  $Mt$  should have a strong negative interfacial Dzyaloshinskii-Moriya interaction.

(vii) The ferromagnet with lowest  $Mt$  should also have the lowest natural (noninteracting) resonance frequency. This frequency depends on  $M$  and the perpendicular anisotropy induced at the interface with the heavy metal.

A system with these characteristics will have a positive optical NR at weak fields, and a negative optical NR at strong fields, which are the necessary conditions to obtain the large change in the nonreciprocity. Additionally, it will also have reversible parallel and antiparallel magnetization states, which can be controlled with applied fields, thus making the change in nonreciprocity controllable. For this system, Pt/Co is a natural choice as the bottom layer with lowest  $Mt$  product due to the strong negative iDMI induced at the interface.

## V. CONCLUSIONS

In conclusion, we have calculated the frequency nonreciprocity induced in propagating Damon-Eshbach spin waves in antiferromagnetically coupled multilayers with interfacial Dzyaloshinskii-Moriya interaction. We have found that the nonreciprocity induced by the iDMI is enhanced in an antiparallel Pt/Co(1.5)/Cu/Co(1.5)/Pt multilayer, opposite to the tendency of canceling out the contributions of opposite interfaces to the iDMI observed in Pt/Co/Pt structures. This is due to the relative orientation of the magnetizations, the direction of propagation of the spin waves, and the sign of the iDMI, effectively adding the contributions of the latter at both Pt interfaces instead of canceling each other out. Furthermore, we have found that in these multilayers, the interplay between the nonreciprocity induced by the iDMI and the interlayer dipolar coupling enhances the nonreciprocity of the optical mode, while decreasing that of the acoustic mode. The opposite effect can be achieved if the Pt layers are replaced with, e.g., Ir, which induces an iDMI of opposite sign. Moreover, we have found that the nonreciprocity of a Pt/Co(1.5)/Cu/Co(2)/Pt multilayer tends to stabilize as the exchange coupling increases because the multilayer behaves as a single thin film with an effective magnetization. We have shown that reversible changes in the nonreciprocity of antiferromagnetically coupled multilayers can be induced through an external applied field due to a transition from antiparallel to parallel magnetization. By selecting appropriately the materials and their thicknesses, we have shown that it is possible to induce changes in the nonreciprocity as high as  $\approx 7$  GHz with fields as low as 130 mT. This is possible by ensuring that the iDMI and dipolar coupling contributions to the nonreciprocity of a given mode have always the same sign, which changes when going from antiparallel to parallel magnetization. We also provide a summary of typical system configurations, which optimize this huge variation in the fre-

quency asymmetry. This change of sign could be of use to invert the direction of the flux of information in nonreciprocal magnonic devices.

## ACKNOWLEDGMENTS

PL. acknowledge financial support from ‘‘Programa de Financiamiento Basal para Centros Científicos y Tecnológicos de Excelencia’’ (Project AFB180001), CEDENNA, CONICYT. Figures 1 and 4 were partially prepared using *Mathematica* 12.0.0.0. We thank R. A. Gallardo for useful discussions on the dynamics of antiferromagnetically coupled bilayers.

## APPENDIX A: DYNAMICAL DIPOLAR FIELDS

In a magnetic multilayer system, the Hamiltonian arising from the dipolar interactions is given by

$$\begin{aligned} \mathcal{H}_d &= -\frac{1}{2} \sum_i \int_{V_i} \vec{M}_i(\vec{r}) \cdot \sum_j \vec{h}_d^j(\vec{r}) d^3r \\ &= -\frac{1}{2} \sum_i \int_{V_i} [\vec{M}_i^{(0)} + \vec{M}_i^{(1)} + \vec{M}_i^{(2)}] \cdot \sum_j \vec{h}_d^{j,(0)} d^3r \\ &\quad - \frac{1}{2} \sum_i \int_{V_i} \vec{M}_i^{(1)} \cdot \sum_j \vec{h}_d^{j,(1)} d^3r, \end{aligned} \quad (\text{A1})$$

where the second and third lines represent the second-order expansion.  $\vec{h}_d^j(\vec{r})$  is the dynamic dipolar field generated by the layer  $j$ .  $\vec{M}_i^{(n)}$  and  $\vec{h}_d^{j,(n)}$  are the  $n$ th-order terms of the expansion of  $\vec{M}_i(\vec{r})$  and  $\vec{h}_d^j(\vec{r})$ , respectively. For  $i = j$ , the dynamical dipolar field is the internal dipolar fields of the layer  $i$ , which has been calculated previously [72,74]. Furthermore, the energy density due to the static component of the dipolar field  $\vec{h}_d^{(0),j}$  between two thin films tends to zero as their size increases [76,83–85]. As we are only interested in the interlayer dipolar interactions ( $i \neq j$ ), (A1) can be rewritten as

$$\mathcal{H}_d^{i \neq j} = -\frac{1}{2} \sum_i \int_{V_i} \vec{M}_i^{(1)}(\vec{r}) \cdot \sum_{j \neq i} \vec{h}_d^{j,(1)}(\vec{r}) d^3r. \quad (\text{A2})$$

Following the same process described in Refs. [73,74], and adopting the coordinate system used in Ref. [72], we calculate the dynamical field  $\vec{h}_d^j(\vec{r})$  in the magnetostatic limit using

$$\vec{h}_d^{j,(1)}(\vec{r}) = -\vec{\nabla} \Phi_j^{(1)}(\vec{r}), \quad (\text{A3})$$

where

$$\nabla^2 \Phi_j^{(1)}(\vec{r}) = \mu_0 \vec{\nabla} \cdot \vec{M}_j^{(1)}(\vec{r}). \quad (\text{A4})$$

The potential can be written in the form

$$\Phi_j^{(1)}(\vec{r}) = \sum_{\vec{k}} \Phi_k^{j,(1)}(Z_j) \exp(i\vec{k} \cdot \vec{r}), \quad (\text{A5})$$

where  $Z_j \equiv Z - Z_j^0$  is the normal coordinate relative to the center of the layer  $j$ .  $Z$  is the absolute perpendicular coordinate shared by all the layers, and  $Z_j^0$  is the value of  $Z$  for the center of the layer  $j$ . From (A4) it can be found that

$$\left[ \frac{\partial^2}{\partial (Z_j)^2} - k^2 \right] \Phi_k^{j,(1)}(Z_j) = f_j(\vec{k}), \quad (\text{A6})$$

where  $f_j(\vec{k})$  is defined below. After taking typical boundary conditions for the magnetic fields, the following solution for the potential is found [72–74]

$$\Phi_k^{j,(1)}(Z_j) = \begin{cases} A_j \exp(-|k|Z_j) & Z_j > t_j/2 \\ a_j \exp(-|k|Z_j) + b_j \exp(|k|Z_j) - \frac{f_j(\vec{k})}{k^2} & -t_j/2 < Z_j < t_j/2, \\ B_j \exp(|k|Z_j) & Z_j < -t_j/2 \end{cases} \quad (\text{A7})$$

where the first line corresponds to  $Z_j^0 < Z_i^0$ , the second line to  $i = j$ , the third to  $Z_j^0 > Z_i^0$ , and

$$\begin{aligned} A_j &= a_j - b_j \exp(|k|t_j) + g_j(\vec{k}) \exp(|k|t_j/2) \\ B_j &= -a_j \exp(|k|t_j) + b_j - g_j(\vec{k}) \exp(|k|t_j/2) \\ a_j &= \frac{1}{2} \exp(-|k|t_j/2) \left[ \frac{f_j(\vec{k})}{k^2} - g_j(\vec{k}) \right] \\ b_j &= \frac{1}{2} \exp(-|k|t_j/2) \left[ \frac{f_j(\vec{k})}{k^2} + g_j(\vec{k}) \right] \\ g_j(\vec{k}) &= \frac{\mu_0}{|k|} \vec{m}_j \cdot \hat{Z} \\ f_j(\vec{k}) &= i\mu_0 \vec{k} \cdot \vec{m}_j, \end{aligned} \quad (\text{A8})$$

where we have used the low-precession angle approximation

$$\vec{M}_j \approx \left( M_j - \frac{1}{2M_j} [(m_x^j)^2 + (m_y^j)^2] \right) \hat{z}_j + \vec{m}_j. \quad (\text{A9})$$

Here,  $\vec{m}_j = m_x^j \hat{x}_j + m_y^j \hat{y}_j$ , and  $\hat{z}_j$  is parallel to the static component of  $\vec{M}_j$ .  $\hat{x}_j$  and  $\hat{y}_j$  form a plane perpendicular to  $\hat{z}_j$ , with  $\hat{y}_j$  lying on the plane of the layer forming an angle  $\varphi_j$  with the  $+X$  axis.  $m_x^j$  and  $m_y^j$  are the dynamical components of the magnetization along the  $\hat{x}_j$  and  $\hat{y}_j$  direction, respectively.

We found that the cases with  $Z_j^0 < Z_i^0$  and  $Z_j^0 > Z_i^0$  have almost identical solutions, and differ only in the sign of  $Z_j$  in a complex exponential. We focus on the solution for  $Z_j^0 < Z_i^0$ , and the solution for  $Z_j^0 > Z_i^0$  is the complex conjugate. This is reflected on the final equations as the  $\text{sgn}(Z_j^0 - Z_i^0)$  function accompanying the imaginary components of the fields. Inserting (A8) into the first line of (A7) we find

$$\Phi_k^{j,(0)}(Z_j) = \frac{\mu_0}{|k|} \sinh\left(\frac{t_j|k|}{2}\right) \left( \vec{m}_j \cdot \hat{Z} - i \frac{\vec{k}}{k} \cdot \vec{m}_j \right) e^{-|k|Z_j} \quad (\text{A10})$$

Inserting Eq. (A10) into (A5), we obtain

$$\Phi_j^{(0)}(\vec{r}) = \sum_{\vec{k}} \frac{\mu_0}{|k|} \sinh\left(\frac{t_j|k|}{2}\right) \left( \vec{m}_j \cdot \hat{z} - i \frac{\vec{k}}{|k|} \cdot \vec{m}_j \right) e^{-|k|Z_j} e^{i\vec{k} \cdot \vec{r}}, \quad (\text{A11})$$

Replacing into (A3), solving the integral (A2), and only keeping second-order terms of the dynamical magnetization, we find the Hamiltonian for the dipolar field generated by the layer  $j$  acting on the layer  $i$

$$\mathcal{H}_{d,\pm}^{i \leftarrow j} = \frac{\mu_0 V_i}{2M_j} \sum_{\vec{k}} \left( H_{x_i x_j}^d m_x^i m_x^j + H_{x_i y_j}^d m_x^i m_y^j + H_{y_i x_j}^d m_y^i m_x^j + H_{y_i y_j}^d m_y^i m_y^j \right) e^{i\vec{k} \cdot \vec{r}}, \quad (\text{A12})$$

where

$$\begin{aligned} H_{x_i x_j}^d &= M_j \zeta_{\text{idc}}^{i,j} [\cos \theta_i \cos \theta_j \cos(\varphi_k - \varphi_i) \cos(\varphi_k - \varphi_j) - \sin \theta_i \sin \theta_j + i (\cos \theta_i \sin \theta_j \cos(\varphi_k - \varphi_i) + \sin \theta_i \cos \theta_j \cos(\varphi_k - \varphi_j))] \\ H_{x_i y_j}^d &= M_j \zeta_{\text{idc}}^{i,j} [\cos \theta_i \cos(\varphi_k - \varphi_i) \sin(\varphi_k - \varphi_j) + i \text{sgn}(Z_i^0 - Z_j^0) \sin \theta_i \sin(\varphi_k - \varphi_j)] \\ H_{y_i x_j}^d &= M_j \zeta_{\text{idc}}^{i,j} [\cos \theta_j \sin(\varphi_k - \varphi_i) \cos(\varphi_k - \varphi_j) + i \text{sgn}(Z_i^0 - Z_j^0) \sin \theta_j \sin(\varphi_k - \varphi_j)] \\ H_{y_i y_j}^d &= M_j \zeta_{\text{idc}}^{i,j} \sin(\varphi_k - \varphi_i) \sin(\varphi_k - \varphi_j). \end{aligned} \quad (\text{A13})$$

Here, we have used

$$\frac{1}{t_i} \int_{-t_i/2+Z_i^0-Z_j^0}^{t_i/2+Z_i^0-Z_j^0} e^{-kZ_j} dZ_j = 2 \frac{\sinh(t_i|k|/2)}{t_i|k|} e^{-|k|\Delta Z_j^i}, \quad (\text{A14})$$

TABLE I. Physical parameters of the Co and Py thin films and their interface with Pt. Throughout this paper, the indexes Co and Py are used to differentiate between both materials when necessary.

|    | $M$ (kA/m) | $A$ (pJ/m) | $t$ (nm) | Interface | $K$ (kJ/m <sup>3</sup> ) | $D$ (mJ/m <sup>2</sup> ) | $J_{\text{eff}}$ (mJ/m <sup>2</sup> ) | $A_s$ (pJ/m) |
|----|------------|------------|----------|-----------|--------------------------|--------------------------|---------------------------------------|--------------|
| Co | 1440       | 31 [77]    | 1.5      | Pt/Co     | 1086 [78,79]             | -1.13 [42]               |                                       |              |
|    |            |            | 1.5      | Co/Pt     | 108 [78,79]              | 0.57 [42,70]             |                                       |              |
|    |            |            | 2.0      | Co/Pt     | 81 [78,79]               | 0.43 [42,70]             | -0.15 [80]                            | -0.14        |
| Py | 637 [40]   | 10 [20,40] | 1.5      | Py/Pt     | 220 [20]                 | -0.13 [20]               |                                       |              |
|    |            |            | 8        | Py/Pt     | 41 [20]                  | -0.02 [20]               |                                       |              |

which arises from taking the average contribution of the dipolar field generated by the layer  $j$  on the layer  $i$ .

### APPENDIX B: EQUILIBRIUM STATE OF THE MAGNETIZATION

The equilibrium state of the magnetization  $\vec{M}_i^0$  is obtained by solving numerically the coupled system of dynamical equations given by the Landau-Lifshitz equation

$$\frac{\partial \vec{M}_i}{\partial t} = -\frac{\gamma}{1+g_i^2} \vec{M}_i \times \vec{H}_{\text{eff}}^i - \frac{\gamma g_i}{(1+\gamma^2)M_i} \vec{M}_i \times (\vec{M}_i \times \vec{H}_{\text{eff}}^i), \quad (\text{B1})$$

where  $g_i$  is the Gilbert damping parameter, and  $\vec{M}_i$  is the magnetization.  $\mu_0 \vec{H}_{\text{eff}}^i = -\partial \mathcal{H} / (V_i \partial \vec{M}_i)$  is the effective field, and  $\mathcal{H}$  is the Hamiltonian of the uniform magnetization given by

$$\mathcal{H} = -\sum_{i=1}^n \left[ \mu_0 \vec{H} \cdot \vec{M}_i V_i + \frac{K_i V_i}{(M_i)^2} [\vec{M}_i \cdot \vec{e}_{K_i}]^2 + \frac{1}{2} \sum_{j=i-1, i+1} \frac{J_{\text{eff}}^{ij} S_{ij}}{M_i M_j} \vec{M}_i \cdot \vec{M}_j - \sum_{j=1}^n \frac{\mu_0}{2} V_i \vec{M}_i \cdot \mathbf{N}_{ij} \cdot \vec{M}_j \right], \quad (\text{B2})$$

where each term represents, respectively, the Zeeman energy, the uniaxial anisotropy, the interlayer exchange coupling, and

the dipolar coupling.  $\vec{e}_{K_i}$  is a unitary vector representing the direction of the easy axis of the anisotropy (taken along the  $Z$  direction), and  $V_i$  is the volume.  $S_{ij}$  is the area of the surface between the layers  $i$  and  $j$ , and  $n$  is the number of magnetic layers of the structure.  $\mathbf{N}_{ij}$  is a rank-3 demagnetizing tensor in the  $XYZ$  reference frame, which relates the shape of the two layers. It is composed of the demagnetizing factors of the layer  $i$  when  $i = j$ , and in the case of thin films all  $\mathbf{N}_{ii}$  elements are approximately zero, with exception of  $N_{ii}^{ZZ} = 1$ . On the other hand, the interlayer demagnetizing tensor ( $i \neq j$ ) is very small in multilayer systems with lateral sizes much larger than their thicknesses [76], and thus the  $k = 0$  contribution of the IDC to the spin wave dispersion is negligible.

### APPENDIX C: PHYSICAL PARAMETERS

Table I shows the physical parameters used in the calculations.  $J_{\text{eff}}$  and  $A_s$  are given for two Co thin films separated by a Cu layer with  $t_{\text{Cu}} = 0.95$  nm [80]. For simplicity, the same  $t_{\text{Cu}}$  and  $J_{\text{eff}}$  are used at the Co/Cu/Py interface. The volume-averaged surface anisotropy constant is  $K_i = K_s^i / t_i$ , where  $K_s^i$  is the surface anisotropy induced at the interface with Pt. Non-identical Pt/Co (bottom) and Co/Pt (top) interfaces [70,71] are taken into account as different  $D$  and  $K$ . Moreover, the thickness of the bottom Co layer always is taken as  $t = 1.5$  nm.

TABLE II. Commonly used abbreviations and mathematical symbols.

| Abbreviation | Meaning   | Symbol           | Meaning   |
|--------------|---|------------------|---|
| HM           | Heavy-Metal   | $i, j$           | Indexes representing each individual layer                  |
| FM           | Ferromagnetic   | $\vec{k}$        | Spin wave vector  |
| P            | Parallel  | $\varphi_k$      | Direction of $\vec{k}$ measured from the $X$ axis           |
| AP           | Antiparallel  | $\vec{k}^{\pm}$  | Spin wave vector with $\varphi_k = \pm\pi/2$                |
| SW           | Spin-wave   | $f_k^{\pm}$      | Frequency of the spin wave with wave vector $\vec{k}^{\pm}$ |
| NR           | Nonreciprocity  | $\Delta f$       | Nonreciprocity $\Delta f = f_k^+ - f_k^-$                   |
| iDMI         | Interfacial Dzyaloshinskii-Moriya interaction   | $H$              | Applied magnetic field                                      |
| iDMI-NR      | Frequency nonreciprocity induced by the interfacial Dzyaloshinskii-Moriya interaction | $M$              | Saturation  |
| IDC          | Interlayer dipolar coupling   | $\vec{M}$        | Direction of the magnetization                              |
| IDC-NR       | Frequency nonreciprocity induced by the interlayer dipolar coupling                   | $\vec{M}^0$      | Equilibrium state of the magnetization                      |
| Acoustic NR  | Nonreciprocity of the acoustic mode   | $\varphi$        | In-plane deviation of $\vec{M}$ relative to the $X$ axis    |
| Optical NR   | Nonreciprocity of the optical mode  | $t$              | Thickness   |
| DE           | Damon-Eschbach  | $D$              | Volume averaged effective iDMI                              |
|              |   | $H_K$            | Perpendicular uniaxial anisotropy field                     |
|              |   | $K$              | Volume averaged magnitude of the anisotropy.                |
|              |   | $J_{\text{eff}}$ | Effective interlayer exchange coupling constant             |

Additionally, and for easier reference, Table II shows a list of abbreviations and mathematical symbols commonly used throughout the discussions within the paper.

## APPENDIX D: INTERLAYER EXCHANGE COUPLING

### 1. Weak coupling

In this section we study the effect of the interlayer exchange coupling on the NR of a Pt/Co(1.5)/Cu/Co(2)/Pt multilayer. Figure 10(a) shows the NR as function of  $J_{\text{eff}}$ . Figures 10(b) and 10(c) show, respectively, the frequency and equilibrium magnetization state. Following we provide a brief description of the observed results, separating the ferromagnetic and the antiferromagnetic exchange coupling:

(i) For antiferromagnetic coupling ( $J_{\text{eff}} < 0$ ) the nonreciprocity of both modes varies slowly as the strength of the coupling increases, with the optical nonreciprocity being stronger than the acoustic.

(ii) For ferromagnetic coupling ( $J_{\text{eff}} > 0$ ) the nonreciprocity tends to stabilize as the multilayer tends towards the behavior of a single magnetic moment (strong  $J_{\text{eff}}$ ) with an effective magnetization  $M_{\text{eff}} = (\pm M_1 t_1 \pm M_2 t_2)/(t_1 + t_2)$ .

(iii) The acoustic nonreciprocity for weak ferromagnetic coupling is stronger than in the antiferromagnetic case. However, it decreases rapidly as the interaction increases.

The last point in particular is in agreement with the results obtained by Bouloussa *et al.* [68], which show that at weak IEC the NR of each mode acts independently if the multilayer is composed of two ferromagnets FM<sub>1</sub> and FM<sub>2</sub>, and that the optical NR tends towards the mean value  $\Delta f = 2\gamma D(t_1 + t_2)k/[\pi(M_1 t_1 + M_2 t_2)]$  for strong IEC.

### 2. Strong coupling

Although the observed behavior is similar to that shown in Ref. [68], there are some key differences, which allow us to provide additional information. In Ref. [68] only one interface has iDMI when two different FMs are studied. This leads to a monotonous decrease of the NR of the acoustic mode as the IEC increases. This is not observed in Fig. 10(a) (the acoustic NR becomes negative and increases in magnitude) due to the additional contribution of the Co/Pt interface. Taking into account that for strong IEC, the bilayer behaves as either a single ferromagnet (for ferromagnetic coupling) or ferrimagnet (with antiferromagnetic coupling) with an effective magnetization, the NR tends toward values given mostly by the iDMI contributions, which are given by

$$\Delta f_{\text{if}} = \frac{\gamma \mu_0}{\pi} \frac{H_{\text{DM}_1} M_1 t_1 + H_{\text{DM}_2} M_2 t_2}{\pm M_1 t_1 \pm M_2 t_2},$$

for the low-frequency mode and

$$\Delta f_{\text{hf}} = \frac{\gamma \mu_0}{\pi} \frac{H_{\text{DM}_2} M_1 t_1 + H_{\text{DM}_1} M_2 t_2}{M_1 t_1 + M_2 t_2},$$

for the high-frequency mode, with  $H_{\text{DM}_i} \equiv 4kD_i/(\mu_0 M_i)$ . The  $\pm$  signs are again taken positive (negative) for magnetization

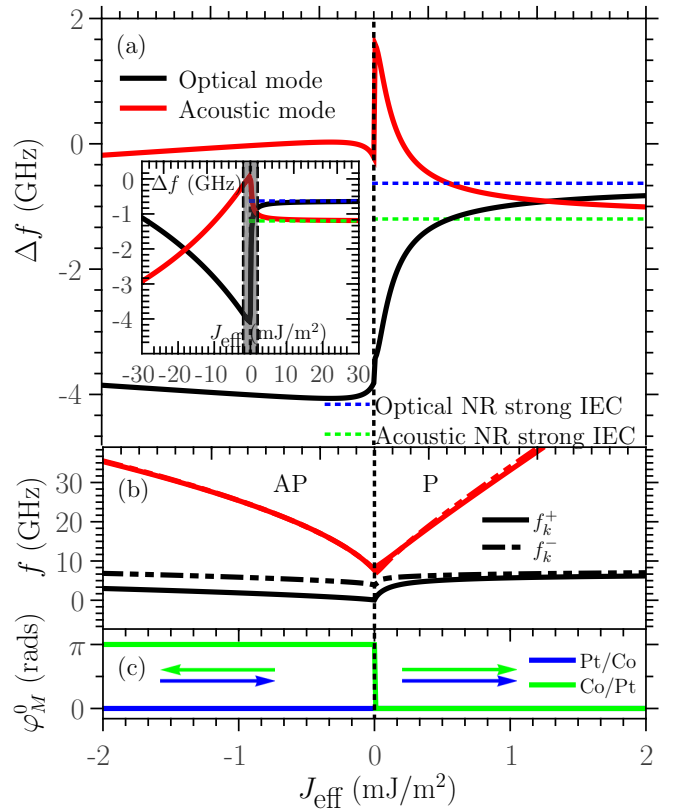


FIG. 10. Behavior of the magnetization of a Pt/Co(1.5)/Cu/Co(2)/Pt multilayer as function of the effective interlayer exchange coupling with fixed wave vector  $k = 16.7 \text{ rad}/\mu\text{m}$ . (a) Frequency nonreciprocity (inset shows the effect of strong interlayer exchange coupling, shadowed region represents the range of  $J_{\text{eff}}$  shown in the main figure), (b) frequency of spin waves propagating in opposite directions, and (c) equilibrium orientation of the magnetization.

along the  $+\hat{X}$  ( $-\hat{X}$ ) direction. Note that when  $M_1 t_1 = M_2 t_2$  these expressions fail in the antiferromagnetic case because  $M_{\text{eff}}$  becomes zero.

For the Pt/Co(1.5)/Cu/Co(2)/Pt multilayer with ferromagnetic IEC, the acoustic iDMI-NR tends towards  $\Delta f_{\text{hf}} = -1.2 \text{ GHz}$  [green dotted line in Fig. 10(a)] and the optical iDMI-NR towards  $\Delta f_{\text{lf}} = -623 \text{ MHz}$  (blue dotted lines). Note that to reach these values, the iDMI-NR of both modes cross each other at  $J_{\text{eff}} \approx 1.1 \text{ mJ/m}^2$ . In the case of strong AFM IEC, the optical iDMI-NR tends towards  $\Delta f_{\text{lf}} = 4.4 \text{ GHz}$  and the acoustic iDMI-NR towards  $\Delta f_{\text{hf}} = -8.4 \text{ GHz}$ . The inset in Fig. 10(a) shows the NR as function of  $J_{\text{eff}}$  for very strong IEC, and it can be observed that the total NR tends to increase, and will eventually stabilize at the iDMI-NR values calculated here. However, typical values of the effective coupling range between  $J_{\text{eff}} = 0.1\text{--}2 \text{ (mJ/m}^2)$ , and the asymptotic values for AFM IEC are only reached well outside of this range.

- [1] D. E. Nikonov and I. A. Young, Overview of beyond-CMOS devices and a uniform methodology for their benchmarking, *Proc. IEEE* **101**, 2498 (2013).
- [2] A. Khitun, M. Bao, and K. L. Wang, Magnonic logic circuits, *J. Phys. D* **43**, 264005 (2010).
- [3] S. A. Wolf, J. Lu, M. R. Stan, E. Chen, and D. M. Treger, The promise of nanomagnetism and spintronics for future logic and universal memory, *Proc. IEEE* **98**, 2155 (2010).
- [4] S. Klingler, P. Pirro, T. Brächer, B. Leven, B. Hillebrands, and A. V. Chumak, Design of a spin-wave majority gate employing mode selection, *Appl. Phys. Lett.* **105**, 152410 (2014).
- [5] S. Klingler, P. Pirro, T. Brächer, B. Leven, B. Hillebrands, and A. V. Chumak, Spin-wave logic devices based on isotropic forward volume magnetostatic waves, *Appl. Phys. Lett.* **106**, 212406 (2015).
- [6] A. V. Chumak, V. I. Vasyuchka, A. A. Serga, and B. Hillebrands, Magnon spintronics, *Nat. Phys.* **11**, 453 (2015).
- [7] I. P. Radu, O. Zografos, A. Vaysset, F. Ciubotaru, J. Yan, J. Swerts, D. Radisic, B. Briggs, B. Soree, M. Manfrini, M. Ercken, C. Wilson, P. Raghavan, S. Sayan, C. Adelman, A. Thean, L. Amaru, P. Gaillardon, G. De Micheli, D. E. Nikonov, S. Manipatruni, and I. A. Young, Spintronic majority gates, in *Proceedings of the 2015 IEEE International Electron Devices Meeting (IEDM)* (IEEE, New York, 2015), pp 32.5.1–32.5.4.
- [8] V. E. Demidov, S. Urazhdin, R. Liu, B. Divinskiy, A. Telegin, and S. O. Demokritov, Excitation of coherent propagating spin waves by pure spin currents, *Nat. Commun.* **7**, 10446 (2016).
- [9] B. Rana and Y. C. Otani, Voltage-Controlled Reconfigurable Spin-Wave Nanochannels and Logic Devices, *Phys. Rev. Appl.* **9**, 014033 (2018).
- [10] Q. Wang, P. Pirro, R. Verba, A. Slavin, B. Hillebrands, and A. V. Chumak, Reconfigurable nanoscale spin-wave directional coupler, *Sci. Adv.* **4**, e1701517 (2018).
- [11] R. Camley, Nonreciprocal surface waves, *Surf. Sci. Rep.* **7**, 103 (1987).
- [12] B. Hillebrands, Spin-wave calculations for multilayered structures, *Phys. Rev. B* **41**, 530 (1990).
- [13] P. Khalili Amiri, B. Rejaei, M. Vroubel, and Y. Zhuang, Nonreciprocal spin wave spectroscopy of thin Ni-Fe stripes, *Appl. Phys. Lett.* **91**, 062502 (2007).
- [14] J. H. Kwon, J. Yoon, P. Deorani, J. M. Lee, J. Sinha, K.-J. Lee, M. Hayashi, and H. Yang, Giant nonreciprocal emission of spin waves in Ta/Py bilayers, *Sci. Adv.* **2**, e1501892 (2016).
- [15] M. Nakayama, K. Yamanoi, S. Kasai, S. Mitani, and T. Manago, Thickness dependence of spin wave nonreciprocity in permalloy film, *Jpn. J. Appl. Phys.* **54**, 083002 (2015).
- [16] F. Ciubotaru, T. Devolder, M. Manfrini, C. Adelman, and I. P. Radu, All electrical propagating spin wave spectroscopy with broadband wavevector capability, *Appl. Phys. Lett.* **109**, 012403 (2016).
- [17] C. S. Chang, M. Kostylev, E. Ivanov, J. Ding, and A. O. Adeyeye, The phase accumulation and antenna near field of microscopic propagating spin wave devices, *Appl. Phys. Lett.* **104**, 032408 (2014).
- [18] K. Di, V. L. Zhang, H. S. Lim, S. C. Ng, M. H. Kuok, X. Qiu, and H. Yang, Asymmetric spin-wave dispersion due to Dzyaloshinskii-Moriya interaction in an ultrathin Pt/CoFeB film, *Appl. Phys. Lett.* **106**, 052403 (2015).
- [19] O. Gladii, M. Haidar, Y. Henry, M. Kostylev, and M. Bailleul, Frequency nonreciprocity of surface spin wave in permalloy thin films, *Phys. Rev. B* **93**, 054430 (2016).
- [20] A. A. Stashkevich, M. Belmeguenai, Y. Roussigné, S. M. Cherif, M. Kostylev, M. Gabor, D. Lacour, C. Tiusan, and M. Hehn, Experimental study of spin-wave dispersion in Py/Pt film structures in the presence of an interface Dzyaloshinskii-Moriya interaction, *Phys. Rev. B* **91**, 214409 (2015).
- [21] K. Di, S. X. Feng, S. N. Piramanayagam, V. L. Zhang, H. S. Lim, S. C. Ng, and M. H. Kuok, Enhancement of spin-wave nonreciprocity in magnonic crystals via synthetic antiferromagnetic coupling, *Sci. Rep.* **5**, 10153 (2015).
- [22] M. Jamali, J. H. Kwon, S.-M. Seo, K.-J. Lee, and H. Yang, Spin wave nonreciprocity for logic device applications, *Sci. Rep.* **3**, 3160 (2013).
- [23] S. Dutta, S.-C. Chang, N. Kani, D. E. Nikonov, S. Manipatruni, I. A. Young, and A. Naemi, Non-volatile clocked spin wave interconnect for beyond-CMOS nanomagnet pipelines, *Sci. Rep.* **5**, 09861 (2015).
- [24] T. Brächer, O. Boule, G. Gaudin, and P. Pirro, Creation of unidirectional spin-wave emitters by utilizing interfacial Dzyaloshinskii-Moriya interaction, *Phys. Rev. B* **95**, 064429 (2017).
- [25] Y. Iguchi, Y. Nii, and Y. Onose, Magneto-electrical control of nonreciprocal microwave response in a multiferroic helimagnet, *Nat. Commun.* **8**, 15252 (2017).
- [26] S. Cheon, H.-W. Lee, and S.-W. Cheong, Nonreciprocal spin waves in a chiral antiferromagnet without the Dzyaloshinskii-Moriya interaction, *Phys. Rev. B* **98**, 184405 (2018).
- [27] A. Savchenko and V. Krivoruchko, Electric-field control of nonreciprocity of spin wave excitation in ferromagnetic nanostripes, *J. Magn. Magn. Mater.* **474**, 9 (2019).
- [28] R. Zivieri, A. Giordano, R. Verba, B. Azzerboni, M. Carpentieri, A. N. Slavin, and G. Finocchio, Theory of nonreciprocal spin-wave excitations in spin hall oscillators with Dzyaloshinskii-Moriya interaction, *Phys. Rev. B* **97**, 134416 (2018).
- [29] S.-W. Cheong, D. Talbayev, V. Kiryukhin, and A. Saxena, Broken symmetries, nonreciprocity, and multiferroicity, *npj Quantum Mater.* **3**, 19 (2018).
- [30] Y. Tokura and N. Nagaosa, Nonreciprocal responses from non-centrosymmetric quantum materials, *Nat. Commun.* **9**, 3740 (2018).
- [31] R. Gallardo, D. Cortés-Ortuño, R. E. Troncoso, and P. Landeros, Spin waves in thin films and magnonic crystals with Dzyaloshinskii-Moriya interactions, in *Three-Dimensional Magnonics Layered, Micro- and Nanostructures* (Jenny Stanford Publishing, Singapore, 2019), pp. 121–160.
- [32] D. D. Stancil and A. Prabhakar, *Spin Waves: Theory and Applications* (Springer, New York, 2009).
- [33] R. L. Melcher, Linear Contribution to Spatial Dispersion in the Spin-Wave Spectrum of Ferromagnets, *Phys. Rev. Lett.* **30**, 125 (1973).
- [34] M. Kataoka, Spin waves in systems with long period helical spin density waves due to the antisymmetric and symmetric exchange interactions, *J. Phys. Soc. Jpn.* **56**, 3635 (1987).
- [35] L. Udvardi and L. Szunyogh, Chiral Asymmetry of the Spin-Wave Spectra in Ultrathin Magnetic Films, *Phys. Rev. Lett.* **102**, 207204 (2009).

- [36] K. Zakeri, Y. Zhang, J. Prokop, T.-H. Chuang, N. Sakr, W. X. Tang, and J. Kirschner, Asymmetric Spin-Wave Dispersion on Fe(110): Direct Evidence of the Dzyaloshinskii-Moriya Interaction, *Phys. Rev. Lett.* **104**, 137203 (2010).
- [37] D. Cortés-Ortuño and P. Landeros, Influence of the Dzyaloshinskii-Moriya interaction on the spin-wave spectra of thin films, *J. Phys.: Condens. Matter* **25**, 156001 (2013).
- [38] J.-H. Moon, S.-M. Seo, K.-J. Lee, K.-W. Kim, J. Ryu, H.-W. Lee, R. D. McMichael, and M. D. Stiles, Spin-wave propagation in the presence of interfacial Dzyaloshinskii-Moriya interaction, *Phys. Rev. B* **88**, 184404 (2013).
- [39] K. Di, V. L. Zhang, H. S. Lim, S. C. Ng, M. H. Kuok, J. Yu, J. Yoon, X. Qiu, and H. Yang, Direct Observation of the Dzyaloshinskii-Moriya Interaction in a Pt/Co/Ni Film, *Phys. Rev. Lett.* **114**, 047201 (2015).
- [40] H. T. Nembach, J. M. Shaw, M. Weiler, E. Jué, and T. J. Silva, Linear relation between heisenberg exchange and interfacial Dzyaloshinskii-Moriya interaction in metal films, *Nat. Phys.* **11**, 825 (2015).
- [41] J. Cho, N.-H. Kim, S. Lee, J.-S. Kim, R. Lavrijsen, A. Solignac, Y. Yin, D.-S. Han, N. J. J. van Hoof, H. J. M. Swagten, B. Koopmans, and C.-Y. You, Thickness dependence of the interfacial Dzyaloshinskii-Moriya interaction in inversion symmetry broken systems, *Nat. Commun.* **6**, 7635 (2015).
- [42] M. Belmeguenai, J.-P. Adam, Y. Roussigné, S. Eimer, T. Devolder, J.-V. Kim, S. M. Cherif, A. Stashkevich, and A. Thiaville, Interfacial Dzyaloshinskii-Moriya interaction in perpendicularly magnetized Pt/Co/AlO<sub>x</sub> ultrathin films measured by brillouin light spectroscopy, *Phys. Rev. B* **91**, 180405(R) (2015).
- [43] V. L. Zhang, K. Di, H. S. Lim, S. C. Ng, M. H. Kuok, J. Yu, J. Yoon, X. Qiu, and H. Yang, In-plane angular dependence of the spin-wave nonreciprocity of an ultrathin film with Dzyaloshinskii-Moriya interaction, *Appl. Phys. Lett.* **107**, 022402 (2015).
- [44] S. Tacchi, R. E. Troncoso, M. Ahlberg, G. Gubbiotti, M. Madami, J. Åkerman, and P. Landeros, Interfacial Dzyaloshinskii-Moriya Interaction in Pt/CoFeB Films: Effect of the Heavy-Metal Thickness, *Phys. Rev. Lett.* **118**, 147201 (2017).
- [45] P. Grünberg, Some ways to modify the spin-wave mode spectra of magnetic multilayers (invited), *J. Appl. Phys.* **57**, 3673 (1985).
- [46] P. Grünberg, R. Schreiber, Y. Pang, M. B. Brodsky, and H. Sowers, Layered Magnetic Structures: Evidence for Antiferromagnetic Coupling of Fe Layers Across Cr Interlayers, *Phys. Rev. Lett.* **57**, 2442 (1986).
- [47] P. X. Zhang and W. Zinn, Spin-wave modes in antiparallel magnetized ferromagnetic double layers, *Phys. Rev. B* **35**, 5219 (1987).
- [48] F. C. Nörtemann, R. L. Stamps, and R. E. Camley, Microscopic calculation of spin waves in antiferromagnetically coupled multilayers: Nonreciprocity and finite-size effects, *Phys. Rev. B* **47**, 11910 (1993).
- [49] M. Mruczkiewicz, P. Graczyk, P. Lupo, A. Adeyeye, G. Gubbiotti, and M. Krawczyk, Spin-wave nonreciprocity and magnonic band structure in a thin permalloy film induced by dynamical coupling with an array of ni stripes, *Phys. Rev. B* **96**, 104411 (2017).
- [50] R. A. Gallardo, P. Alvarado-Seguel, T. Schneider, C. Gonzalez-Fuentes, A. Roldán-Molina, K. Lenz, J. Lindner, and P. Landeros, Spin-wave nonreciprocity in magnetization-graded ferromagnetic films, *New J. Phys.* **21**, 033026 (2019).
- [51] R. A. Gallardo, T. Schneider, A. K. Chaurasiya, A. Oelschlägel, S. S. P. K. Arekapudi, A. Roldán-Molina, R. Hübner, K. Lenz, A. Barman, J. Fassbender, J. Lindner, O. Hellwig, and P. Landeros, Reconfigurable Spin-Wave Nonreciprocity Induced by Dipolar Interaction in a Coupled Ferromagnetic Bilayer, *Phys. Rev. Appl.* **12**, 034012 (2019).
- [52] E. Albisetti, S. Tacchi, R. Silvani, G. Scaramuzzi, S. Finizio, S. Wintz, C. Rinaldi, M. Cantoni, J. Raabe, G. Carlotti, R. Bertacco, E. Riedo, and D. Petti, Optically inspired nanomagnonics with nonreciprocal spin waves in synthetic antiferromagnets, *Adv. Mater.* **32**, 1906439 (2020).
- [53] V. Sluka, T. Schneider, R. A. Gallardo, A. Kákay, M. Weigand, T. Warnatz, R. Mattheis, A. Roldán-Molina, P. Landeros, V. Tiberkevich, A. Slavin, G. Schütz, A. Erbe, A. Deac, J. Lindner, J. Raabe, J. Fassbender, and S. Wintz, Emission and propagation of 1d and 2d spin waves with nanoscale wavelengths in anisotropic spin textures, *Nat. Nanotechnol.* **14**, 328 (2019).
- [54] J. A. Otálora, M. Yan, H. Schultheiss, R. Hertel, and A. Kákay, Curvature-Induced Asymmetric Spin-Wave Dispersion, *Phys. Rev. Lett.* **117**, 227203 (2016).
- [55] A. V. Sadovnikov, E. N. Beginin, S. E. Sheshukova, Y. P. Sharaevskii, A. I. Stognij, N. N. Novitski, V. K. Sakharov, Y. V. Khivintsev, and S. A. Nikitov, Route toward semiconductor magnonics: Light-induced spin-wave nonreciprocity in a YIG/GaAs structure, *Phys. Rev. B* **99**, 054424 (2019).
- [56] I. Dzyaloshinsky, A thermodynamic theory of “weak” ferromagnetism of antiferromagnetics, *J. Phys. Chem. Solids* **4**, 241 (1958).
- [57] T. Moriya, Anisotropic superexchange interaction and weak ferromagnetism, *Phys. Rev.* **120**, 91 (1960).
- [58] A. Fert and P. M. Levy, Role of Anisotropic Exchange Interactions in Determining the Properties of Spin-Glasses, *Phys. Rev. Lett.* **44**, 1538 (1980).
- [59] A. Fert, V. Cros, and J. Sampaio, Skyrmions on the track, *Nat. Nanotechnol.* **8**, 152 (2013).
- [60] M. Bode, M. Heide, K. von Bergmann, P. Ferriani, S. Heinze, G. Bihlmayer, A. Kubetzka, O. Pietzsch, S. Blügel, and R. Wiesendanger, Chiral magnetic order at surfaces driven by inversion asymmetry, *Nature (London)* **447**, 190 (2007).
- [61] N. Nagaosa and Y. Tokura, Topological properties and dynamics of magnetic skyrmions, *Nat. Nanotechnol.* **8**, 899 (2013).
- [62] C. Moreau-Luchaire, C. Moutafis, N. Reyren, J. Sampaio, C. A. F. Vaz, N. Van Horne, K. Bouzehouane, K. Garcia, C. Deranlot, P. Warnicke, P. Wohlhüter, J.-M. George, M. Weigand, J. Raabe, V. Cros, and A. Fert, Additive interfacial chiral interaction in multilayers for stabilization of small individual skyrmions at room temperature, *Nat. Nanotechnol.* **11**, 444 (2016).
- [63] W. Jiang, P. Upadhyaya, W. Zhang, G. Yu, M. B. Jungfleisch, F. Y. Fradin, J. E. Pearson, Y. Tserkovnyak, K. L. Wang, O. Heinonen, S. G. E. te Velthuis, and A. Hoffmann, Blowing magnetic skyrmion bubbles, *Science* **349**, 283 (2015).
- [64] S. Emori, U. Bauer, S.-M. Ahn, E. Martinez, and G. S. D. Beach, Current-driven dynamics of chiral ferromagnetic domain walls, *Nat. Mater.* **12**, 611 (2013).

- [65] K.-S. Ryu, L. Thomas, S.-H. Yang, and S. Parkin, Chiral spin torque at magnetic domain walls, *Nat. Nanotechnol.* **8**, 527 (2013).
- [66] A. Fernández-Pacheco, E. Vedmedenko, F. Ummelen, R. Mansell, D. Petit, and R. P. Cowburn, Symmetry-breaking interlayer Dzyaloshinskii-Moriya interactions in synthetic antiferromagnets, *Nat. Mater.* **18**, 679 (2019).
- [67] M. T. Birch, D. Cortés-Ortuño, L. A. Turnbull, M. N. Wilson, F. Groß, N. Träger, A. Laurensen, N. Bukin, S. H. Moody, M. Weigand, G. Schütz, H. Popescu, R. Fan, P. Steadman, J. A. T. Verezhak, G. Balakrishnan, J. C. Loudon, A. C. Twitchett-Harrison, O. Hovorka, H. Fangohr, F. Y. Ogrin, J. Gräfe, and P. D. Hatton, Real-space imaging of confined magnetic skyrmion tubes, *Nat. Commun.* **11**, 1726 (2020).
- [68] H. Bouloussa, Y. Roussigné, M. Belmeguenai, A. Stashkevich, S. M. Chérif, J. Yu, and H. Yang, Spin-wave calculations for magnetic stacks with interface Dzyaloshinskii-Moriya interaction, *Phys. Rev. B* **98**, 024428 (2018).
- [69] M. Ishibashi, Y. Shiota, T. Li, S. Funada, T. Moriyama, and T. Ono, Switchable giant nonreciprocal frequency shift of propagating spin waves in synthetic antiferromagnets, *Sci. Adv.* **6**, eaaz6931 (2020).
- [70] A. Hrabec, N. A. Porter, A. Wells, M. J. Benitez, G. Burnell, S. McVitie, D. McGrouther, T. A. Moore, and C. H. Marrows, Measuring and tailoring the Dzyaloshinskii-Moriya interaction in perpendicularly magnetized thin films, *Phys. Rev. B* **90**, 020402(R) (2014).
- [71] S.-G. Je, D.-H. Kim, S.-C. Yoo, B.-C. Min, K.-J. Lee, and S.-B. Choe, Asymmetric magnetic domain-wall motion by the Dzyaloshinskii-Moriya interaction, *Phys. Rev. B* **88**, 214401 (2013).
- [72] A. F. Franco and P. Landeros, Ferromagnetic resonance of a heterogeneous multilayer system with interlayer exchange coupling: An accessible model, *J. Phys. D* **49**, 385003 (2016).
- [73] R. Arias and D. L. Mills, Extrinsic contributions to the ferromagnetic resonance response of ultrathin films, *Phys. Rev. B* **60**, 7395 (1999).
- [74] P. Landeros, R. E. Arias, and D. L. Mills, Two magnon scattering in ultrathin ferromagnets: The case where the magnetization is out of plane, *Phys. Rev. B* **77**, 214405 (2008).
- [75] A. Aharoni, *Introduction to the Theory of Ferromagnetism* (Oxford University Press, Oxford, 1996).
- [76] A. F. Franco, Intensity enhancement of ferromagnetic resonance modes in exchange coupled magnetic multilayers, *New J. Phys.* **22**, 013017 (2020).
- [77] G. Bertotti, *Hysteresis in Magnetism for Physicist, Materials Scientists, and Engineers* (Academic Press, New York, 1998).
- [78] S. Bandiera, R. C. Sousa, B. Rodmacq, and B. Dieny, Asymmetric interfacial perpendicular magnetic anisotropy in Pt/Co/Pt trilayers, *IEEE Magn. Lett.* **2**, 3000504 (2011).
- [79] T. Y. Lee, Y. C. Won, D. S. Son, S. H. Lim, and S. Lee, Strength of perpendicular magnetic anisotropy at bottom and top interfaces in [Pt/Co/Pt] trilayers, *IEEE Magn. Lett.* **5**, 1 (2014).
- [80] S. S. P. Parkin, R. Bhadra, and K. P. Roche, Oscillatory Magnetic Exchange Coupling through Thin Copper Layers, *Phys. Rev. Lett.* **66**, 2152 (1991).
- [81] S. Li, Q. Li, J. Xu, S. Yan, G.-X. Miao, S. Kang, Y. Dai, J. Jiao, and Y. Lü, Tunable optical mode ferromagnetic resonance in FeCoB/Ru/FeCoB synthetic antiferromagnetic trilayers under uniaxial magnetic anisotropy, *Adv. Func. Mater.* **26**, 3738 (2016).
- [82] H. Yang, A. Thiaville, S. Rohart, A. Fert, and M. Chshiev, Anatomy of Dzyaloshinskii-Moriya Interaction at Co/Pt Interfaces, *Phys. Rev. Lett.* **115**, 267210 (2015).
- [83] M. Buchmeier, B. K. Kuanr, R. R. Gareev, D. E. Bürgler, and P. Grünberg, Spin waves in magnetic double layers with strong antiferromagnetic interlayer exchange coupling: Theory and experiment, *Phys. Rev. B* **67**, 184404 (2003).
- [84] P. Vargas and D. Altbir, Dipolar effects in multilayers with interface roughness, *Phys. Rev. B* **62**, 6337 (2000).
- [85] A. F. Franco, J. L. Déjardin, and H. Kachkachi, Ferromagnetic resonance of a magnetic dimer with dipolar coupling, *J. Appl. Phys.* **116**, 243905 (2014).